Article

Topology and Emergent Symmetries in Dense Compact Star Matter

Yong-Liang Ma [1,2,*] and Wen-Cong Yang [1,2]

1   College of Physics, Jilin University, Changchun 130012, China
2   School of Fundamental Physics and Mathematical Sciences, Hangzhou Institute for Advanced Study, UCAS, Hangzhou 310024, China
*   Correspondence: ylma@ucas.ac.cn

Abstract: It has been found that the topology effect and the possible emergent hidden scale and hidden local flavor symmetries at high density reveal a novel structure of compact star matter. When $N_f \geq 2$, baryons can be described by skyrmions when the number of color N_c is regarded as a large parameter and there is a robust topology change—the transition from skyrmion to half-skyrmion—in the skyrmion matter approach to dense nuclear matter. The hidden scale and local flavor symmetries, which are sources introducing the scalar meson and vector mesons, are significant elements for understanding the nuclear force in nonlinear chiral effective theories. We review in this paper how the robust conclusions from the topology approach to dense matter and emergent hidden scale and hidden local flavor symmetries figure in generalized nuclear effective field theory (GnEFT), which is applicable to nuclear matter from low density to compact star density. The topology change encoded in the parameters of the effective field theory is interpreted as the hadron-quark continuity in the sense of the Cheshire Cat Principle. A novel feature predicted in this theory that has not been found before is the precocious appearance of the conformal sound velocity in the cores of massive stars, although the trace of the energy-momentum tensor of the system is not zero. That is, there is a pseudoconformal structure in the compact star matter and, in contrast to the usual picture, the matter is made of colorless quasiparticles of fractional baryon charges. A possible resolution of the longstanding g_A quench problem in nuclei transition and the compatibility of the predictions of the GnEFT with the global properties of neutron star and the data from gravitational wave detections are also discussed.

Keywords: dense nuclear matter; topology change; scale symmetry; quantum Hall droplet; gravitational wave

1. Introduction

Although it has been investigated for several decades, there is no consensus on how to describe the equation of state (EoS) of dense nuclear matter relevant to compact stars [1–8]. We do not know with certainty what the constituents involved are and how the symmetries of quantum chromodynamics (QCD) evolve in medium. The resolution of these questions has strong impacts on the most fundamental issues of particle and nuclear physics that have defied theorists, for example, the mechanism of chiral symmetry breaking and the emergence of nucleon mass.

In the past decade, we studied dense nuclear matter using a generalized nuclear effective field theory (GnEFT) including the lowest-lying iso-vector vector mesons ρ and iso-scalar vector meson ω and the lightest iso-scalar scalar meson σ, in addition to the nucleon and pion considered in the standard chiral effective field theory (SχEFT) [9–12]. Implemented with the robust conclusions of the medium modified hadron properties obtained from the topology structure of QCD at large N_c limit, we found that at the density relevant to the cores of massive stars, the sound velocity saturates the approximate

conformal limit although the scale symmetry is not restored and the system is still in the confined phase [13,14]. That is, there could be a pseudoconformal structure in the cores of massive stars (see Refs. [5,7,15–18] for reviews). Although it was previously believed that the sound velocity in massive neutron stars should deviate from the conformal limit [19–22], this saturation is now observed in more and more models [23–27] and allowed by the constraints from neutron star data [28,29].

To obtain the pseudoconformal structure of dense nuclear matter, two significant ingredients are considered in the GnEFT, the hidden symmetries which are invisible in the matter-free space—hidden scale symmetry and hidden local flavor symmetry—and the topology of QCD at large N_c.

The hidden local flavor symmetry—hidden local symmetry (HLS) [30–32]—provides an effective field theory (EFT) approach of vector mesons ρ and ω in the framework where the chiral symmetry is realized in a nonlinearized pattern. Furthermore, the breaking scale symmetry offers a source for introducing the scalar meson—regarded as dilaton—in the EFTs à la Crewther and Tunstall [33–35]. In the compact star matter, due to the strong correlations among its constituents, these hidden symmetries may emerge and these emergent symmetries affect the compact star properties in either a direct or an indirect way.

When considered in the large N_c limit, the baryon can be regarded as the topology soliton—skyrmion—in a nonlinear field theory of mesons [36]. This is an alternative approach to nuclear physics different from the currently widely used models including the nucleon as an explicit fermionic field. Using the skyrmion approach, it was found that when the nuclear matter is squeezed to a certain high density, the constituent of the nuclear matter is changed from a baryon number-1 object to a baryon number-1/2 object, i.e., there is a topology change [37,38]. The existence of this topology change is robust although the density where it happens—denoted as $n_{1/2}$—is model-dependent [39–44]. An interesting conclusion which has not been observed in all the other approaches is that, after $n_{1/2}$, some hadron properties such as the pion decay constant in medium f_π^* and effective nucleon mass m_N^* become density-independent [42,43]. Moreover, it was found that at $n \gtrsim n_{1/2}$, the sound velocity saturates the conformal limit $v_s^2/c^2 \simeq 1/3$ [45] although f_π^* and m_N^* are not zero.

Since the skyrmion approach to nuclear matter requires tremendous numerical simulations and includes obscure mathematics, the approach to nuclear matter using the EFTs including baryon fields as explicit degrees of freedom are widely used now. We implement the model-independent observations from the skyrmion approach and the effects of the emergent symmetries with the medium-modified parameters in GnEFT through (extended) Brown–Rho scaling [46]. By using the model-independent low momentum interaction, called the V_{lowk} approach, and implementing the strategy of Wilsonian renormalization group flow [47–49] with respect to the constraints from the nuclear matter around saturation density $n_0 \approx 0.16$ fm^{-3}, we construct the equation of state (EoS) of compact star matter which has pseudoconformal symmetry, i.e., the sound velocity in the compact star matter satisfies the conformal limit $v_s^2/c^2 \simeq 1/3$ but the conformal symmetry is still breaking since the trace of the energy-momentum tensor (TEMT) is not zero. The predictions of the pseudoconformal model (PCM) satisfy all constraints from terrestrial experiments and astrophysical observations.

In this contribution, complementing [5,7,15–18], we will review the key points of the pseudoconformal structure of dense nuclear matter with a special interest on the emergent scale, local symmetries and topology constituents of compact star matter.

2. Hidden Symmetries and Hadron Resonances

In the SχEFT of nuclear physics, the hadron degrees of freedom are nucleons and pions. However, it has been recognized long ago that the hadron resonances are crucial for reproducing the empirical data of nuclear matter around saturation density, such as the iso-scalar scalar meson σ and the iso-vector vector mesons ρ and iso-scalar vector ω in the Walecka model [50].

Another reason to include the hadron resonances in GnEFT is that although the finite nuclei as well as infinite nuclear matter can be studied by using the nuclear EFTs—"pionless or pionful"—anchored on relevant symmetries fairly accurately, these nuclear EFTs are expected to break down at some high densities relevant to, say, the interiors of massive stars. For example, when applying the SχEFT to nuclear matter where power counting happens in terms of $O(k_F^q)$ with k_F being the fermi momentum, it was found that even for normal nuclear matter, the expansion requires going to $\sim q = 5$ [2]. Therefore, more loops should be considered and more parameters are involved. This makes the calculation involved and the ambiguities hard to control.

With the above considerations in mind, we include the iso-scalar scalar meson σ and vector mesons ρ and ω in GnEFT and expect that GnEFT can appropriately describe nuclear matter from low to the compact star density at a low order. Note that it was recently found that the iso-vector scalar mesons δ (denoted as $a_0(980)$ in particle physics) also affects the EoS through the symmetry energy in a considerable way [51,52]. However, since we do not have any idea of how to construct an EFT for them and since their structures are still under debate, we will not consider them in the present work.

In the literature, the hidden symmetries which are not visible in the matter-free space provide sources for including hadron resonances in the effective theories. Explicitly, the observed hadron resonances list in the particle data group booklet [53] indicate that the approximate chiral symmetry in QCD breaks to the vector channel and pions can be regarded as the Nambu–Goldstone bosons of the broken axial symmetry. The local flavor symmetry—hidden local symmetry (HLS) [30–32]—suggests an EFT approach of vector mesons in the framework where the chiral symmetry is broken to the vector channel. And, the hidden scale symmetry offers a source for introducing the iso-scalar scalar meson to chiral EFTs á la Crewther and Tunstall [33,34]. In the compact star matter, due to the strong correlations among its constituents, these hidden symmetries may emerge and these emergent symmetries affect the compact star properties in either a direct or an indirect way.

2.1. Hidden Scale Symmetry

The QCD Lagrangian in the chiral limit preserves scale symmetry. Therefore, the trace of the momentum-energy tensor θ_μ^μ vanishes at classical level, i.e., $\langle \theta_\mu^\mu \rangle = 0$. This invariance is broken by trace anomaly at quantum level

$$\theta_\mu^\mu = \frac{\beta(\alpha_s)}{4\alpha_s} G_{\mu\nu}^a G^{a\mu\nu} + (1 + \gamma_5) \sum_{q=u,d,s} m_q \bar{q} q, \tag{1}$$

where m_q is the quark mass. Since the trace anomaly has the quantum number of vacuum, it has long been taken as the source of the iso-scalar scalar meson in effective models [33,34,54–56].

In the construction of the effective models of the iso-scalar scalar meson using the trace anomaly as its source, the only constraint on the effective Lagrangian comes from the anomaly matching. However, to build an EFT of the scalar meson à la Weinberg, one should set up the power counting mechanism. This was finalized in the pioneering work of Crewther and Tunstall (CT for short) [33,34].

An alternative to the CT scheme is the framework proposed by Golterman and Shamir (GS) in the large N_c and large N_f Veneziano limit [57]. Although the IR structure is presumably different in both approaches, the GS scheme and CT scheme were found to be of the same form to NLO once β' in CT and $\Delta n_f = |n_f^c - n_f|$ in GS are related. In this work, we follow the CT scheme.

The basic idea of Crewther and Tunstall is that the iso-scalar scalar meson can be regarded as the pseudo-Nambu–Goldstone boson generated by the spontaneous breaking of the scale symmetry. Provided that there is a nonperturbative infrared fixed point (IRFP) α_{IR} in QCD, the mass of the scalar meson, here dilaton, is generated by the explicit scale symmetry breaking which is encoded in the departure from the IRFP and the current

quark mass. The magnitude of the mass is proportional to the deviation from the IRFP ($\Delta\alpha = \alpha_{IR} - \alpha_s$) and the current quark mass therefore the situation is very similar to the chiral perturbation theory where the masses of the Nambu–Goldstone bosons are proportional to the current quark masses which measure the magnitude of the explicit chiral symmetry breaking. Note that whether the nonperturbative IRFP which the CT approach is anchored on exists in QCD is not yet confirmed. Among a variety of approaches, we simply refer to the positive arguments given in [58–60]. Moreover, the lattice QCD indicates that, in the thermal system, the scale symmetry may exists in the IR region and this therefore leads to the existence of massless glueballs [61]. It seems not strange to expect such a scale invariance to emerge in medium.

Following the procedure of CT [33,34], introducing the conformal compensator field χ which has the scale dimension 1 and $\langle\theta^\mu_\mu\rangle = \langle\chi^4\rangle = f^4_\chi$, one can write the chiral-scale effective Lagrangian. The power counting of the Lagrangian is in terms of momentum (derivative), quark mass—as what is used in the standarded chiral perturbation theory—and $\Delta\alpha = \alpha_{IR} - \alpha_s$ due to the departure from the IRFP

$$\mathcal{O}(p^2) \sim \mathcal{O}(m_q) \sim \mathcal{O}(\Delta\alpha). \tag{2}$$

In terms of the pseudoscalar pions $U(x) = e^{2i\pi(x)/f_\pi}$ and $\chi = e^{\sigma(x)/f_\chi}$ with σ being the dilaton field which will be identified with the lightest scalar meson $f_0(500)$, one can write the effective Lagrangian at leading chiral-scale order as

$$\mathcal{L}_{\text{LO}} = \mathcal{L}^{d=4}_{\text{inv}} + \mathcal{L}^{d>4}_{\text{anom}} + \mathcal{L}^{d<4}_{\text{mass}} \tag{3}$$

where d stands for the scale dimension and

$$\begin{aligned}
\mathcal{L}^{d=4}_{\text{inv}} &= c_1 \frac{f^2_\pi}{4}\left(\frac{\chi}{f_\chi}\right)^2 \text{Tr}\left(\partial_\mu U\partial^\mu U^\dagger\right) + \frac{1}{2}c_2\partial_\mu\chi\partial^\mu\chi \\
&\quad + c_3\left(\frac{\chi}{f_\chi}\right)^4,
\end{aligned} \tag{4a}$$

$$\begin{aligned}
\mathcal{L}^{d>4}_{\text{anom}} &= (1-c_1)\frac{f^2_\pi}{4}\left(\frac{\chi}{f_\chi}\right)^{2+\beta'} \text{Tr}\left(\partial_\mu U\partial^\mu U^\dagger\right) \\
&\quad + \frac{1}{2}(1-c_2)\left(\frac{\chi}{f_\chi}\right)^{\beta'}\partial_\mu\chi\partial^\mu\chi \\
&\quad + c_4\left(\frac{\chi}{f_\chi}\right)^{4+\beta'},
\end{aligned} \tag{4b}$$

$$\mathcal{L}^{d<4}_{\text{mass}} = \frac{f^2_\pi}{4}\left(\frac{\chi}{f_\chi}\right)^{3-\gamma_m} \text{Tr}\left(\mathcal{M}^\dagger U + U^\dagger\mathcal{M}\right), \tag{4c}$$

where $\mathcal{M}$ stands for the current quark mass matrix with $\mathcal{M} = \text{diag}(m^2_\pi, m^2_\pi, 2m^2_K - m^2_\pi)$, γ_m is the anomalous dimension of the quark mass operator $\bar{q}q$, and the c_i's are unknown constants. It should be noted that, differently from chiral perturbation theory, c_3 and c_4 have scale-chiral order $O(p^2)$ since, as will be seen later, they are proportional to the dilaton mass square, similarly to $\mathcal{M}$ for the pseudo-scalar Nambu–Goldstone mesons.

We next consider the dilaton potential $V(\chi)$

$$V(\chi) = -c_3\left(\frac{\chi}{f_\chi}\right)^4 - c_4\left(\frac{\chi}{f_\chi}\right)^{4+\beta'}. \tag{5}$$

The saddle point equation in the matter-free space yields

$$V(\chi) = -(4+\beta')c\left(\frac{\chi}{f_\chi}\right)^4 + 4c\left(\frac{\chi}{f_\chi}\right)^{4+\beta'}, \tag{6}$$

where

$$c = -\frac{1}{4}c_4 = \frac{1}{4+\beta'}c_3 > 0. \tag{7}$$

We see that, when $\beta' \neq 0$, that is, the second term in (5) is not scale-invariant, the dilaton potential is in the Nambu–Goldstone (NG) mode with minima at $\langle \chi \rangle = f_\chi$. However, if $\beta' = 0$, $V(\chi) = 0$ and the dilaton potential is scale-invariant, the scale symmetry does not break spontaneously. This β' dependence of the scale symmetry breaking tells us that the spontaneous breaking of scale symmetry is locked to the explicit breaking of scale symmetry and the former is triggered by the latter. Therefore, unlike chiral symmetry, spontaneous breaking of scale symmetry cannot take place in the absence of explicit symmetry breaking [62–64]. We refer to this as the "Freund–Nambu theorem".

Using the definition of the dilaton mass m_σ, from the dilaton potential (6) one obtains

$$c = \frac{m_\sigma^2 f_\chi^2}{4\beta'(4+\beta')}. \tag{8}$$

so that the constant c and therefore c_3 and c_4 through relation (7) have chiral-scale dimension $O(p^2)$ since $c \propto m_\sigma^2$. We finally obtain the dilaton potential as

$$V(\chi) = \frac{m_\sigma^2 f_\chi^2}{4\beta'(4+\beta')}\left(\frac{\chi}{f_\chi}\right)^4\left[-(4+\beta') + 4\left(\frac{\chi}{f_\chi}\right)^{\beta'}\right]. \tag{9}$$

When $\beta' \ll 1$, the dilaton potential is approximated to [65]

$$V(\chi) = \frac{m_\sigma^2 f_\chi^2}{4}\left(\frac{\chi}{f_\chi}\right)^4\left(\ln\frac{\chi}{f_\chi} - \frac{1}{4}\right). \tag{10}$$

This yields the scale Ward–Takahashi identity

$$\langle \theta_\mu^\mu \rangle = \langle \partial_\mu D^\mu \rangle = -\frac{m_\chi^2}{4f_\chi^2}\langle \chi^4 \rangle \tag{11}$$

which is the partially conserved dilatonic current (PCDC) relation, the counterpart to the PCAC for the pion.

Along the reasoning of CT, one can set up a systematic higher-order expansion and write down the higher-order terms [66,67]. In the general Lagrangian, there are so many unknown parameters that it is difficult to give any prediction in practice, even at the leading order. However, one can make substantial progress and arrive at a manageable form by taking the so called "leading-order scale symmetry (LOSS)" approximation that corresponds to

$$c_1 \approx c_2 \approx 1. \tag{12}$$

That is, in LOSS, the scale symmetry breaking—in the chiral limit—is lodged entirely in the dilaton potential $V(\chi)$. The resulting Lagrangian is

$$\mathcal{L}_{\text{LO}}^{\chi\text{limit}} = \frac{f_\pi^2}{4}\left(\frac{\chi}{f_\chi}\right)^2 \text{Tr}\left(\partial_\mu U \partial^\mu U^\dagger\right) + \frac{1}{2}\partial_\mu \chi \partial^\mu \chi - V(\chi). \tag{13}$$

Whether the LOSS approximation is valid cannot be justified from the first principle. The numerical analysis shows that it works for light nuclei [68,69] and compact star matter [5] but it violates around the saturation density [70]. In this contribution, without specification, we work with LOSS.

2.2. Hidden Local Flavor Symmetry

To include the vector mesons into the chiral effective theory we use, among a variety of approaches, hidden local symmetry (HLS) [30–32]. Explicitly, considering the chiral symmetry $G_{\text{global}} = [SU(2)_L \times SU(2)_R]_{\text{global}}$, following the convention of [32], we decompose the field $U(x)$ as

$$U(x) = \xi_L^\dagger \xi_R(x). \tag{14}$$

Therefore, one can sandwich a local unitary transformation $H_{\text{local}} = [U(2)_V]_{\text{local}}$ between this decomposition. Under transformation $G_{\text{global}} \times H_{\text{local}}$, $\xi_{L,R}$ transform as

$$\xi_{L,R}(x) \mapsto \xi'_{L,R}(x) = h(x)\xi_{L,R}(x)g^\dagger_{L,R}, \tag{15}$$

where $h(x) \in H_{\text{local}}$ and $g_{L,R} \in SU(2)_{L,R}$. The variables $\xi_{L,R}$ can be parameterized as

$$\xi_{L,R}(x) = e^{i\sigma(x)/(2f_\sigma)}e^{\pm i\pi(x)/(2f_\pi)}, \tag{16}$$

where $\pi(x) = \pi^a X^a$ and $\sigma(x) = \sigma^\alpha S^\alpha$ with X^a are the generators of the broken chiral symmetry and S^a are the generators of the unbroken subgroup H. Note that here σ is the Nambu–Goldstone boson which becomes the longitudinal part of the gauge boson V_μ of symmetry H_{local} after the spontaneous breaking of the HLS, with f_σ being its decay constant.

With quantities $\xi_{L,R}$ one can define the following two 1-forms:

$$\hat{\alpha}_{\|\mu} = \frac{1}{2i}(D_\mu\xi_R \cdot \xi_R^\dagger + D_\mu\xi_L \cdot \xi_L^\dagger),$$
$$\hat{\alpha}_{\perp\mu} = \frac{1}{2i}(D_\mu\xi_R \cdot \xi_R^\dagger - D_\mu\xi_L \cdot \xi_L^\dagger), \tag{17}$$

where the covariant derivative is defined as $D_\mu\xi_{R,L} = (\partial_\mu - iV_\mu)\xi_{R,L}$. Both $\hat{\alpha}_{\|}^\mu$ and $\hat{\alpha}_\perp^\mu$ transform covariantly under the full symmetry G_{global}, i.e., $\hat{\alpha}_{\|,\perp}^\mu \to h(x)\hat{\alpha}_{\|,\perp}^\mu h(x)^\dagger$. Moreover, the field strength tensor $V_{\mu\nu}$ of the gauge field V_μ

$$V_{\mu\nu}(x) = \partial_\mu V_\nu(x) - \partial_\nu V_\mu(x) - i[V_\mu(x), V_\nu(x)], \tag{18}$$

also has the covariant transformation $V_{\mu\nu}(x) \to h(x)V_{\mu\nu}(x)h(x)^\dagger$.

In terms of $\hat{\alpha}_{\|,\perp}^\mu$ defined by Equation (17) and $V_{\mu\nu}$ given in (18), the most general effective Lagrangian with the minimal number of derivatives in the chiral limit can be written as

$$\mathcal{L}_{\text{HLS}} = f_\pi^2 \text{Tr}[\hat{\alpha}_{\perp\mu}\hat{\alpha}_\perp^\mu] + f_\sigma^2 \text{Tr}[\hat{\alpha}_{\|\mu}\hat{\alpha}_\|^\mu] - \frac{1}{2g^2}\text{Tr}[V_{\mu\nu}V^{\mu\nu}]. \tag{19}$$

One can easily check that, in the unitary gauge which will be taken in this paper,

$$\xi_L^\dagger = \xi_R \equiv \xi = e^{i\pi/(2f_\pi)}, \quad U(x) = \xi^2(x), \tag{20}$$

the gauge bosons V_μ acquire mass at the classical level

$$m_V^2 = m_\rho^2 = m_\omega^2 = g^2 f_\sigma^2, \tag{21}$$

which has the standard form of the gauge boson mass from the Higgs mechanism.

So far, we use $H_{\text{local}} = [U(2)_V]_{\text{local}}$, and therefore the rho meson and omega meson have the same mass (21). This approximation works well in the matter-free space. However, in medium, it is found that this approximation breaks [9,71] and it is reasonable to take the HLS $H_{\text{local}} = [SU(2)_V \times U(1)_V]_{\text{local}}$.

In the HLS, considering that the masses of ρ mesons are smaller than the scale Λ_χ of the chiral symmetry breaking, one can make a systematic expansion including vector meson loops due to the gauge invariance [72,73] and set up a self-consistent power counting mechanism, the essential character of effective theory [32]. Since in the nuclear matter, due to the strong correlation among hadrons, the effective mass of the ρ meson is reduced, the convergence of the expansion is enhanced.

Based on the Wilsonian renormalization group (RG) approach, it has been found that there is a vector manifestation (VM) fixed point in the hidden local symmetry (HLS) at high energy scales, i.e., $f_\pi \to 0$ and $m_\rho \to m_\pi \to 0$ in the chiral limit [32,74]. It is straightforward to expect that the VM also exists at (super-)high density. We will see later that this VM, although it happens at the super high density beyond the cores of massive stars, affects the equation of the state of neutron star matter in an indirect way.

Moreover, using dilaton compensated chiral effective theory, it was found that there is a dilaton limit fixed point (DLFP) in the dense baryonic matter, that is, the medium-modified dilaton decay constant $f_\chi^* \to 0$ at high density [71,75]. When the DLFP is approached, the vector meson ρ becomes massless and the HLS emerges [76]. Although the DLFP is saturated at a density beyond the core of massive neutron stars $\sim 10\ n_0$, it affects the properties of the equation of state of the neutron star, for example the sound velocity [9,10,77].

3. Topology Change and Hadron-Quark Continuity

It was recognized long ago that in the large N_c limit, baryon properties share the same N_c scaling as the soliton properties in nonlinear mesonic theories [78]. This gives an alternative approach to nuclear physics by using the topology properties of QCD at large N_c limit, that is, regarding the baryon as a skyrmion in the Skyrme model [36], in contrast to the standard EFT approach that includes the baryon fields as explicit degrees of freedom.

Using the skyrmion approach and regarding baryon as skyrmion, one can study the single baryon, multibaryon and nuclear matter in a unified way [44,79,80]. Since the skyrmion approach is only based on the topology structure of QCD, some qualitative conclusions obtained in this approach, such as the existence of the topology change and density dependence of some parameters in nuclear matter that will be illustrated later, should be model-independent.

3.1. Baryons as Topology Objects and Topology Change

When the chiral symmetry is realized in a nonlinear pattern, the Nambu–Goldstone boson of the spontaneous breaking of chiral symmetry, pion, is expressed in the polar parameterization through the unitary field $U(x)$ satisfying $U(x)U(x)^\dagger = U(x)^\dagger U(x) = 1$. Hence, for any fixed time, say, t_0, the static configuration $U(\mathbf{x}, t_0)$ defines a map from the manifold R^3 to the manifold S^3 in the isospin space, that is

$$U(\mathbf{x}, t_0) : R^3 \to S^3. \tag{22}$$

At low energy limit, QCD goes to the vacuum, i.e.,

$$U(|\mathbf{x}| \to \infty, t_0) \ = \ \mathbf{1}, \tag{23}$$

therefore, all the points at $|\mathbf{x}| \to \infty$ are mapped onto the north pole of S^3 and the energy of the system is finite.

In terms of the terminology of topology, maps (22) constitute the third homotopy group $\pi_3(S^3) \sim Z$ where the integer Z accounts for the times that S^3 is covered by the mapping $U(\mathbf{x}, t_0)$, i.e., winding numbers. When the time coordinate is changed—regarded as a homotopy trasformation—the winding number is conserved since the field configurations in homotopically distinct classes cannot transit. In Skyrme-type models where the chiral field $U(x)$ figures, the conserved winding number represents the conserved baryon number in QCD and the baryon arises as a topological soliton. Therefore, in the construction of

Skyrme-type models, only the unitarity of the chiral field $U(x)$ and the condition (23) are essential characteristics that should be taken into account [44].

In the skyrmion approach, in addition to the single baryon and multi-baryon systems, one can also access the nuclear matter. By putting skyrmions onto the crystal lattice and change the crystal size such that the density effect enters, the skyrmion matter—regarded as nuclear matter—is simulated [81]. This approach suggests a method for studying nuclear matter at densities higher than the dilute density using the topology of QCD. In practice, we do not know which crystalline structure nature favors. So far, the face-centered-cubic (FCC) crystal is the known configuration that yields the lowest energy [37,38].

In the skyrmion crystal approach to dense nuclear matter, several novel phenomena that have not been observed in other frameworks, including baryon fields as explicit degrees of freedom, as mean field theory and the density functional approach have revealed. Among them, the most important one is the existence of half-skyrmion—a winding number-1/2 object—configurations at some higher density. Since the prediction of the half-skyrmion is anchored on the topology of QCD, its presence is robust and does not depend on what degrees of freedom other than the pions are involved [82]. The significant point is that the nuclear matter involves a topology change from skyrmions to half-skyrmions when density is increased to a certain value $n_{1/2} \gtrsim 2n_0$, and this topology change is responsible for a dramatic change in the properties of dense nuclear matter. We will see that it plays significant roles in describing the equation of state for compressed baryonic matter relevant for massive compact stars.

Figure 1 shows how the skyrmion FCC crystal configuration transforms to the half-skyrmion configuration in terms of the distribution of baryon number density. In the left panel, one can easily see that besides the corners and the center of the square where the skyrmions are originally placed, the baryon number density emerges at the middles of the lines connecting the corners. That is, in the half-skyrmion matter, the half-skyrmions form the CC crystal. After integration, each blue area has winding number-1/2 (for a detailed explanation, see, e.g., Ref. [83]).
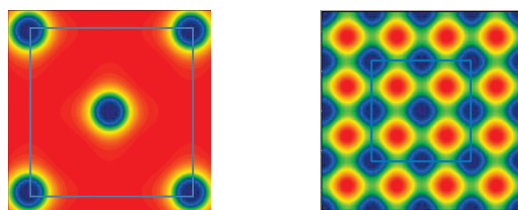

Figure 1. The distribution of the baryon number density (the blue areas) in the skyrmion (**left panel**) matter and half-skyrmion matter (**right panel**). The crystal size 2 L is denoted by the blue quare.

Due to this topology change, a variety of novel phenomena which have not been observed in the standard nucleon EFT approach emerge. Although the locations of the density $n_{1/2}$ where these phenomena start depend on the model, their existences are model-independent. Some of them which closely relate to the present review are summarized as follows:

- Quark condensate: In skyrmion matter, the space-average of the normalized quark condensate $\phi_0 = \frac{1}{2}\text{Tr}(U)$ is

$$\langle\phi_0\rangle = \frac{1}{V}\int_0^{2L} d^3x \frac{1}{2}\text{Tr}(U), \tag{24}$$

  with V being the volume of the crystal cell. It is found that in the skyrmion matter $\langle\phi_0\rangle \neq 0$ but $\langle\phi_0\rangle \to 0$ in the half-skyrmion state. This implies that the quark condensate in medium—here in skyrmion matter— $\langle\bar{q}q\rangle^* \to 0$ in the half-skyrmion matter when space-averaged.

- Pion decay constant: In the skyrmion crystal approach, it is found that the medium modified pion decay constant f_π^* first decreases with density until $n_{1/2}$ but after $n_{1/2}$ f_π^* stays as a constant. We plot a typical result of f_π^* as a function of crystal size calculated by using the HLS up to the next leading order including the homogeneous Wess–Zumino terms [84] in Figure 2. This means that in the half-skyrmion matter, although the space-averaged quark condensate vanishes, the chiral symmetry is not restored and it is still in the Nambu–Goldstone mode. Actually, in the half-skyrmion matter, the inhomogeneous quark condensate persists [85].

- Nucleon mass: By using the medium modified pion decay constant f_π^*, one can calculate the density dependence of nucleon mass m_N^* and obtain the scaling relation

$$\frac{m_N^*}{m_N} \approx \frac{f_\pi^*}{f_\pi},\tag{25}$$

which, as discussed later, is consistent with the Brown–Rho scaling from the LOSS [46]. It is found that, as shown in Figure 2, similar to f_π^*, m_N^*—regarded as soliton mass M_{sol}^* in the large N_c limit—first decreases with density until $n_{1/2}$, after which it stays as a constant. This is predominantly, if not entirely, due to the space-averaged quark condensate going to zero at $n_{1/2}$. Since in the half-skyrmion matter, $\langle \bar{q}q \rangle^* \to 0$, this observation indicates that the nucleon mass has decomposition

$$m_N = m_0 + \Delta(\bar{q}q),\tag{26}$$

that is, there is a chiral invariant part in the nucleon mass and the parity doubling of nucleons may emerge in dense nuclear matter [86,87].
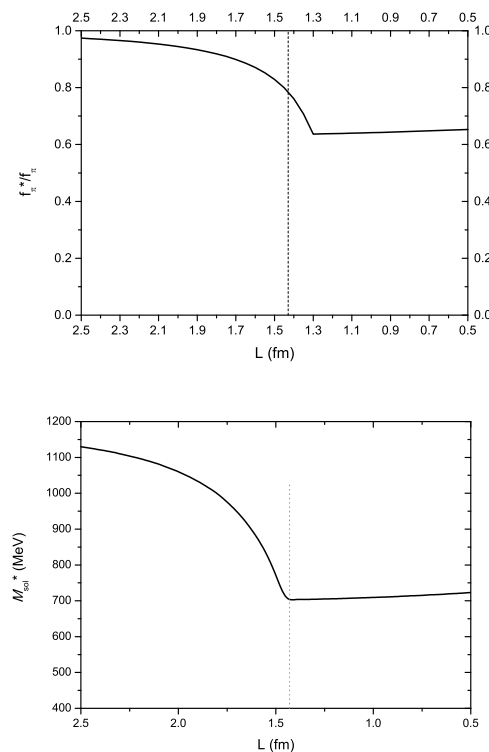

Figure 2. Typical results of the medium modified f_π^* and m_N^* vs. lattice size L calculated from the FCC crystal by using the HLS up to the next leading order including the Wess–Zumino terms [84]. The vertical line denotes the location of the normal nuclear matter density in the FCC crystal.

We want to emphasize that the tendencies discussed above are robust but the location of $n_{1/2}$ is highly model-dependent. So far, we cannot pin down the value of $n_{1/2}$. The

combination of the terrestrial experiments and astrophysical observations leads to the constraint, as shown later, that $2.0n_0 \lesssim n_{1/2} \lesssim 4.0n_0$.

3.2. Topological Baryon for $N_f = 1$

As stated above, the skyrmion approach is anchored on the map (22). How to or whether it is possible to study a baryon such as Δ resonance in one-flavor QCD using the topology approach is a problem since $\pi_3(U(1)) = 0$. In the one-flavor case, the degree of freedom in the nonlinear theory of the meson is the iso-scalar meson η' which is dominated by the axial $U(1)$ anomaly. Therefore, the soliton construction of the baryon no longer applies since, for instance, the standard topological charge—the winding number—cannot be identified.

In 2018, Komargodski [88] noted that the chiral effective theory for one-flavor QCD has a conserved topological current $J_{\alpha\beta\gamma} = \epsilon_{\alpha\beta\gamma\lambda}\partial^\lambda \eta'/2\pi$ which is carried by $(2+1)$-dimensional charged sheets with the η' field undergoing a 2π jump across the sheet. When these sheets have finite boundaries, which is physically valid, they can carry massless edge excitations with quantum baryon numbers; the baryon therefore can be identified with fast spinning baryons These sheets are described by a topological field theory through a level-rank duality argument [89–91], very similar to the situation of the fractional quantum Hall (FQH) effect [92].

By using the HLS approach, Karasik [93] pointed out that the vector mesons play the role of the Chern–Simons vector fields living on the QHD that forms the $N_f = 1$ baryon. This proposal gives a unified picture for the two types of baryons and allows them to continuously transform one to the other. Recently, Bigazzi et al proposed a string theory description of the quantum Hall (QH) sheet using the Witten–Sakai–Sugimoto model [94].

3.3. Cheshire Cat Principle and Quark-Hadron Continuity

Based on what we discussed above and will develop below, it is found that the topology change is significant for developing the pseudo-conformal model (PCM) of dense nuclear matter, especially for the existence of the conformal sound velocity in compact star matter. Because of this topology change, there is a cusp structure in the symmetry energy E_{sym} [11,95] which provides a simple mechanism for the putative soft-to-hard change in the EoS for compact stars at $n \sim 2n_0$ needed to account for the observed massive neutron stars with mass $\sim 2M_\odot$. In the models that resort to the hadron-quark continuity in terms of the specific quark degrees of freedom that are strongly coupled, the hardening of the EoS at $n \gtrsim 2n_0$ is associated with "deconfinement" of quarks [4,23]. The question is whether or how the topology change represents the "quark deconfinement" process. Here, we provide a conjecture on this issue.

We first consider one-flavor QCD in which, as we discussed above, the topological baryon an be interpreted as the fractional Quantum Hall (FQH) droplet [88]. In this case, the connection between the topology change and the quark deconfinement can be made by using the Cheshire Cat mechanism [96].

Explicitly, we consider a $(2+1)$-dimensional chiral bag surrounding a QH droplet as shown in Figure 3. The bag is an annulus of width $2R$ clouded by an η' with a monodromy of 2π. The bag is filled in by N_c quarks. When the bag radius shrinks to zero, the chiral bag reduces to a vortex string with unit baryon number—the simile is left.

It is shown that a current transverse to the smile—the x direction—embodying the Callan–Harvey anomaly outflow [97] appears. This transverse current is analogous to the Hall current of the QH effect through the emergence of an effective $U(1)$ gauge field. This $U(1)$ gauge field which is described by a purely topological field theory in $(2+1)$ dimensions lives in the disk enclosed by the Cheshire Cat smile and the action of the emergent $U(1)$ gauge field is of an FQH droplet. The quantum numbers of this baryon—as a QH droplet—follow from the construction of the chiral bag. This argument can be extended to the case where $N_f = 2, 3$ that we are concerned with in this review.
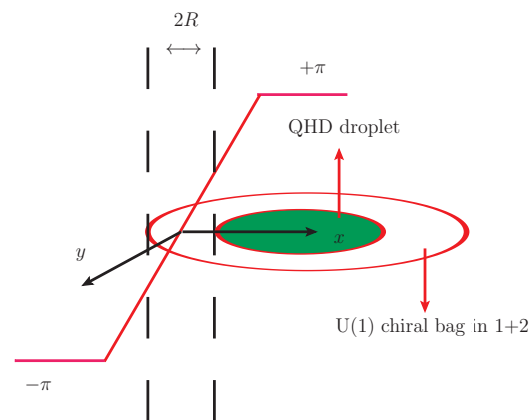
Figure 3. Chiral bag (annulus) in $(1 + 2)$-dimension surrounding a QH droplet (green sheet) [96].

Now suppose the η' becomes lighter at higher density as is expected at high temperature [98]. Then the FQH pancakes could become relevant as density increases and figure in dense matter in a form of a stack of FQH pancakes. Interactions must then induce the N_c quarks with the fractional $(1/N_c)$ baryon charge living on the boundary of the pancakes to tunnel between the pancakes. This could lead to sheets of fractional baryon-charged topological objects in $(3 + 1)$ dimensions. In fact, in a recent analysis of dense matter using the skyrmion crystal approach, certain configurations unstable at low density but stabilized at high density of sheets with half-baryon charged objects called "lasagnes" were found [99]; this was also the case with $1/q$-charged baryons in tube configurations with baryons living on the surface of the tube [100]. In addition, it was recently found that this QHD sheet exists in the string theory description of single-flavor QCD [94]. Anyway, it seems not impossible that the layers of FQH droplets in $(3 + 1)$ dimensions give rise to deconfined quasiparticles dual to quarks of fractional charges, e.g., half-skyrmions, and this FQH droplet may be explored in superdense compact star matter [101]. Such deconfinement can take place in the presence of domain walls as in some condensed matter systems [102] and the half-skyrmions probed in the density regime $n > n_{1/2}$ could be deconfined as in the Néel-VBS deconfined quantum critical transition [102,103].

4. Generalized Nuclear Effective Field Theory

Equipped with the discussion of the hidden symmetries, one can write down the generalized nuclear effective field theory (GnEFT). Here, for simplicity, we only consider the leading order scale symmetry (LOSS). In this limit, the effective Lagrangian is expressed as

$$\mathcal{L}_{GnEFT} = \mathcal{L}^M_{GnEFT} + \mathcal{L}^B_{GnEFT} - V(\chi) \tag{27}$$

where

$$
\begin{aligned}
\mathcal{L}^M_{GnEFT} &= f_\pi^2 \left(\frac{\chi}{f_\sigma}\right)^2 \mathrm{Tr}\left[\hat{\alpha}_{\perp\mu}\hat{\alpha}_\perp^\mu\right] \\
&\quad + a f_\pi^2 \left(\frac{\chi}{f_\sigma}\right)^2 \mathrm{Tr}\left[\hat{\alpha}_{\parallel\mu}\hat{\alpha}_\parallel^\mu\right] - \frac{1}{2g^2}\mathrm{Tr}\left(V_{\mu\nu}V^{\mu\nu}\right) \\
&\quad - \frac{1}{2}\partial_\mu\chi\partial^\mu\chi, \\
\mathcal{L}^B_{GnEFT} &= \bar{N}i\gamma_\mu D^\mu N - \frac{\chi}{f_\sigma}m_0\bar{N}N \\
&\quad + g_A \bar{N}\gamma_\mu\gamma_5\hat{\alpha}_\perp^\mu N + g_V \bar{N}\gamma_\mu\hat{\alpha}_\parallel^\mu N, \\
V(\chi) &= h_5\left(\frac{\chi}{f_\sigma}\right)^4 + h_6\left(\frac{\chi}{f_\sigma}\right)^{4+\beta'},
\end{aligned}
\tag{28}
$$

with N being the iso-doublet of the baryon fields. Using the saddle-point equation and in terms of the dilaton mass m_σ, the dilaton potential is reexpressed as

$$V(\chi) = \frac{m_\sigma^2 f_\chi^2}{\beta'(4+\beta')} \left(\frac{\chi}{f_\chi}\right)^4 \left[\left(\frac{\chi}{f_\chi}\right)^{\beta'} - \left(1 + \frac{\beta'}{4}\right)\right]. \tag{29}$$

Lagrangian (27) is the starting point of the PCM of the compact star matter.

4.1. Generalized Brown–Rho Scaling

From GnEFT, one can derive the generalized BR scaling [46] which mimics the medium-modified hadron properties at LOSS. The most general scaling including the corrections to LOSS can be found in [104]. At LOSS, one finds

$$\frac{f_\pi^*}{f_\pi} = \frac{m_V^*}{m_V} = \frac{m_N^*}{m_N} = \Phi(n), \quad \frac{m_\sigma^*}{m_\sigma} = \Phi(n)^{1+\beta'}, \tag{30}$$

where $\Phi(n) = \langle\chi\rangle^*/\langle\chi\rangle$. The density effect entering through BR scaling is inherited from QCD at the scale where the GnEFT and QCD are matched (denoted as IDD). We will see later that when we perform the V_{lowk} calculation, there is an induced density dependence (DD$_{indueced}$) due to the correlations among nucleons. The full density dependence in our final results is the sum of them, IDD+DD$_{indueced}$.

Note that, differently from the BR scaling originally proposed in [46], here, the density scaling of the sigma mass depends on β'. When $\beta' \ll 1$, the dilaton potential reduces to the logarithm form [66] and the scaling of sigma mass becomes $m_\sigma^*/m_\sigma \to \Phi(n)$, the form suggested in [46].

So far, we do not have any priority to fix β' without ambiguity. What we have learned is that when using the chiral-scale EFT to study dense skyrmion matter, β' is constrained to $1 \lesssim |\beta'| \lesssim 3.5$ [45,105]. This magnitude is consistent with the phenomenological Lagrangian approach to nuclear matter where the six-point interaction of the sigma meson—roughly $\beta' = 2$ in the present framework—was found to be significant [87].

It should be noted that the scaling relation (30) is obtained from the LOSS. In the following explicit calculation, to fit the nuclear matter properties around saturation density n_0, we should tune the scaling parameters, which is attributed to the corrections to LOSS.

4.2. Quenching of g_A in Nuclei Transition

Let us put the discussion of compact star matter aside for a moment. We show how the scale symmetry manifests in nuclei by looking at the g_A quench problem in the nuclear Gamow–Teller transitions, that is, the axial coupling constant $g_A^{\text{free}} = 1.276$ in the vacuum should be taken as $g_A^{\text{eff}} \to 1$ in the nuclear Gamow–Teller transitions [106–108]. Some uncertainties in experiments and possible ambiguities in theoretical resolutions weer discussed in [109] recently. Here I follow the reasoning of [68–70].

In GnEFT, the axial current relevant to the nuclear Gamow–Teller transitions is generally expressed as

$$q_{\text{SSB}} g_A \bar{\psi} \tau^+ \gamma_\mu \gamma_5 \psi \tag{31}$$

where

$$q_{\text{SSB}} = c_A + (1 - c_A) \Phi^{\beta'}. \tag{32}$$

In the matter-free space or very low density, $\Phi \to 1$ so that $q_{\text{SSB}} \to 1$, that is, scale symmetry breaking does not affect the effective axial coupling. In nuclear medium, since $\Phi < 1$, the axial coupling becomes modified when $c_A < 1$ since $\beta' \neq 0$ and the trace anomaly effect enters. Using (31), the quench factor is finally expressed as [70]

$$q_{\text{GnEFT}}^{\text{ESPM}} = q_{\text{SSB}} \times q_{\text{SNC}}, \tag{33}$$

where q_{SNC} accounts for strong nuclear many-body correlations. By using the Fermi-liquid fixed point theory [110], one can work out q_{SNC} [68]. With the value $\Phi(n_0) \simeq 0.8$ [111], one obtains [70]

$$q_{SNC} \simeq 0.79. \tag{34}$$

In nucleus up to $A \sim 60$, g_A^{eff} in the shell model calculation of the nuclear Gamow–Teller transitions turn out to be [107,108]

$$g_A^{\text{eff}} = q_{\text{light}} g_A^{\text{free}} = 0.98\text{–}1.18 \tag{35}$$

with $g_A^{\text{free}} = 1.276$. In the range $q_{\text{light}} = 0.76\text{–}0.93$ implied by this equation, let us pick what gives $g_A^{\text{eff}} \simeq 1$

$$q_{\text{light}} \simeq 0.78. \tag{36}$$

With respect to (34), one concludes that $q_{SSB} \simeq 1$ in Equation (34). This indicates that $\Phi \simeq 1$ in the light nuclei system and the axial current is scale-symmetric.

However, as the mass number of nuclei goes up above $A \sim 60$, the scenario is different. A more stringent recent experiment from RIKEN on the superallowed GT decay of the doubly magic nucleus ^{100}Sn [112] yields [70]

$$q_{\text{RIKEN}}^{\text{ESPN}} = 0.46\text{–}0.55. \tag{37}$$

This means that, if the RIKEN data are right, in the heavy nuclei system, (34) is not enough to account for the quench factor. This discrepancy can be interpreted by assuming $c_A \simeq 0.15$ and $\beta' \simeq 2.5$, which is consistent with the estimation from the resolution of the HWZ problem [45,105]. This choice gives

$$q_{SSB} = 0.64 \tag{38}$$

which leads to

$$q_{GnEFT}^{\text{ESPM}} = q_{SSB} \times q_{SNC} = 0.64 \times 0.79 \simeq 0.5 \tag{39}$$

consistent with the constraint from the RIKEN data (37).

The simple analysis above teaches us the following lessons: in light nuclei and very low density nuclear matter, conformal symmetry emerges [113,114]. However, in normal nuclear matter, such conformal symmetry is absent. Later, we will see that at high density approaching the dilaton-limit fixed point (DLFP), this symmetry reappears. This tells us how the scale symmetry manifests in nuclear system.

The key reasoning made in the above argument is that the Fermi-liquid fixed-piont (FLFP) calculation can be identified with the Extreme Single Particle Model (ESPM). If this identifiction is problematic, the above argument should be taken with cautioun [109].

5. Equation of State of Nuclear Matter

Let us come back to the nuclear matter properties by using the GnEFT with the generalized BR scaling (30). Since the GnEFT includes, in addition to the Nambu–Goldstone bosons pions, the effects from the hadron resonances σ, ρ and ω, the obtained equation of state is expected to be applicable to the cores of massive stars up to, i.e., $\sim 10n_0$.

Considering that the density dependence of the medium-modified hadron properties is categorized into two regions due to the topology change delimited by density $n_{1/2}$, we denote the region $n < n_{1/2}$ as R-I and region $n > n_{1/2}$ as R-II in the parameterization of the density effect. The density scalings of the medium-modified hadron properties are summarized as follows:

- R-I: In this region, the scaling function Φ in the master formulism (30) decreases with density. Without first principle information on the explicit form of Φ, we parameterize it as

$$\Phi_I = \frac{1}{1 + c_I \frac{n}{n_0}} \tag{40}$$

with c_I being a constant. With respect to the nuclear matter properties around saturation density [16] and the measured pion decay constant [111], the range of c_I is found to be

$$c_I \approx 0.13\text{–}0.20. \tag{41}$$

In practice, to reproduce the nuclear matter properties around saturation density, it is easy to imagine that there should be fine-tuning within the range (41).

- R-II: Due to the topology change—which is one of the most robust inputs from skyrmion matter—at $n_{1/2} \gtrsim 2n_0$, the scaling behaviours of some parameters in R-II are drastically different from that in R-I. The scaling behaviours of the parameters are quite involved.

  - g_ρ and ρ mass: The hidden local gauge coupling g_ρ related to the ρ mass through the KSRF relation. Combined with the vector manifestation(VM) fixed-point structure of HLS this leads to the fact that for $n > n_{1/2}$ the coupling g_ρ should drop to zero toward the putative VM fixed point n_{VM}. We take the simple form [77]

$$\frac{g^*_{\rho NN}}{g_{\rho NN}} = \begin{cases} 1 - 0.1\frac{n}{n_0}, & \text{for } n \in (n_{1/2}, 3.5n_0) \\ 0.65 - h\frac{(n - 3.5n_0)}{n_0}, & \text{for } n \in (3.5n_0, n_{VM}) \end{cases} \tag{42}$$

    where h is determined by the location of the VM fixed point $m^*_\rho/m_\rho = g^*_{\rho NN}/g_{\rho NN} \to 0$, e.g., $h \approx 0.04$ for $n_{VM} \approx 20n_0$. Where n_{VM} is located is not known in QCD. In compact stars, whether it is $\sim 6n_0$ or $\gtrsim 20n_0$ does not make noticeable differences with one possible exception, namely, the star sound velocity, as we will see below.

  - Nucleon mass: As we learned from the 1/2-skyrmion phase, the parity doubling emerges giving rise to the chiral-invariant mass m_0, and the pion decay constant f^*_π becomes density invariant. In the chiral-scale effective theory, they both lock to the dilaton condensate f^*_χ. Therefore we have

$$\frac{m^*_N}{m_N} \approx \frac{f^*_\chi}{f_\chi} \approx \frac{f^*_\pi}{f_\pi} \equiv \kappa \sim (0.6 - 0.9). \tag{43}$$

  - Dilaton mass: Since from the partially conserved dilatation current (PCDC) the dilaton mass is also proportional to the dilaton condensate [33], we then have

$$\frac{m^*_\sigma}{m_\sigma} \approx \kappa. \tag{44}$$

  - ω meson: The nuclear matter density dependences of the ω meson properties are subtle. Using the HLS, the ω mass is locked to the hidden gauge coupling constant. Since the $U(2)$ HLS which works well in R-I breaks in R-II [9,71], some sort of fine-tuning is needed in the density-scaling of ω mass and hidden gauge coupling constant. We take it as

$$\frac{m^*_\omega}{m_\omega} \approx \kappa\frac{g^*_\omega}{g_\omega} = \kappa\Phi_\omega(n). \tag{45}$$

In the numerical calculation, we take

$$\Phi_\omega \equiv \frac{g_\omega^*}{g_\omega} \approx 1 - d\,\frac{n - n_{1/2}}{n_0} \tag{46}$$

with $d \approx 0.05$.

After the above discussions, one can make a numerical calculation of the equation of state of the nuclear matter by using the renormalization-group approach with V_{lowk} (V_{lowk} RG) [9,115] once the vacuum values of the parameters are fixed.

The V_{lowk} RG is extracted from an effective low-mementum T-matrix, T_{lowk}, which is obtained by imposing a cutoff Λ—the nucleons with momentum $k \leq \Lambda$ are considered but the $k > \Lambda$ compoents are integrated out—on all the loop integrals in the T-matrix equation and replace the bare V_{NN} with an effective potential V_{lowk}. By requiring that the observables are independent of the scale Λ, the renormalization flow of V_{lowk} can be obtained. We refer to [47–49] for the details of the V_{lowk}RG and to [9] for its application to chiral-scale EFT which GnEFT is anchored on.

Therefore, after taking the V_{lowk} approach, the meson fluctuation effects are taken into account and the density effect in the results comes from both the intrinsic density dependence encoded in the BR scaling (IDD) and hadron correlations (DD$_{induced}$). It is found that, with the only parameter c_I, all the nuclear matter properties $n \leq 2n_0 \lesssim n_{1/2}$ can be reproduced well [16].

The density $n_{1/2}$ where the topology change happens and how the R-I and R-II are delineated changes the density dependence of the hadron properties drastically and therefore impacts the EoS in a qualitative way. However, as we discussed above, the location of the topology change is model-dependent so that we cannot pin down its value theoretically. With respect to the constraints from various astrophysical observations available so far, the maximum mass of a neutron star and the gravitational wave data, we constrain $n_{1/2}$ as $2.0n_0 \lesssim n_{1/2} \lesssim 4.0n_0$ [12].

5.1. Vector Manifestation

Where the vector manifestation fixed point $n_{\rm VM}$ is located is known neither theoretically nor empirically. While most of the global properties of compact stars do not seem to depend much on where $n_{\rm VM}$ lies since its value is above the possible central density of massive compact stars, it seems that it affects the sound velocity of compact star matter in an indirect way.

Here, to show the effect of $n_{\rm VM}$ on the sound velocity, we fix the typical value $n_{1/2} = 2.5\,n_0$. We choose the typical values $n_{\rm VM} = 6.75\,n_0$ and $20\,n_0$ in Equation (42). The lower value of the density is about the central density of massive stars, and the upper value represents an "asymptotic density" where perturbative QCD is expected to be applicable. The $n_{\rm VM}$ dependences of the sound velocity are plotted in Figure 4.

From Figure 4, one can easily see that the location of $n_{\rm VM}$ drastically affects the behavior of sound velocity. When $n_{\rm VM}$ is big, the sound velocity converges to the "conformal velocity" $v_s^2 \approx 1/3$ after $n_{1/2}$. However, for a smaller $n_{\rm VM}$, e.g., $n_{\rm VM} \approx 7\,n_0$, it increases steadily after $n_{1/2}$ and overshoots conformal velocity. We will see later that the conformal sound velocity is locked to the (pseudo-)conformality of matter.

5.2. Pseudoconformal Structure

Now, let us understand what the implication of the conformal velocity in nuclear matter is.

In the matter system, the sound velocity is defined by

$$v_s^2 = \frac{\partial P(n)}{\partial n} \Big/ \frac{\partial \epsilon}{\partial n}, \tag{47}$$

where ϵ and P are, respectively, the energy density and the pressure density. We then have

$$\int \frac{\partial P(n)}{\partial n} dn = \int v_s^2 \frac{\partial \epsilon}{\partial n} dn - \frac{1}{3} C_0 \tag{48}$$

where C_0 is a constant independent of density and the factor $\frac{1}{3}$ is due to convenience. For a constant sound velocity, one obtains

$$P(n) = v_s^2 \epsilon(n) - \frac{1}{3} C_0. \tag{49}$$

And for $v_s^2 / c^2 = 1/3$, we obtain

$$\epsilon(n) - 3P(n) = C_0. \tag{50}$$

For an ideal liquid system where the nuclear matter is assumed to work, the TEMT is expressed as

$$\theta_\mu^\mu = \epsilon - 3P. \tag{51}$$

Therefore, when $v_s^2 / c^2 = 1/3$, one has

$$\langle \theta_\mu^\mu \rangle = C_0, \tag{52}$$

which is a density-independent quantity. When $C_0 = 0$, the TEMT vanishes so that the scale symmetry in the system is restored. A system with this property can be regarded as one where both the scale symmetry and chiral symmetry are restored, quarks are deconfined and perturbative QCD applies. Since this scenario happens at a density much beyond that in the cores of massive stars, we are not interested in it.
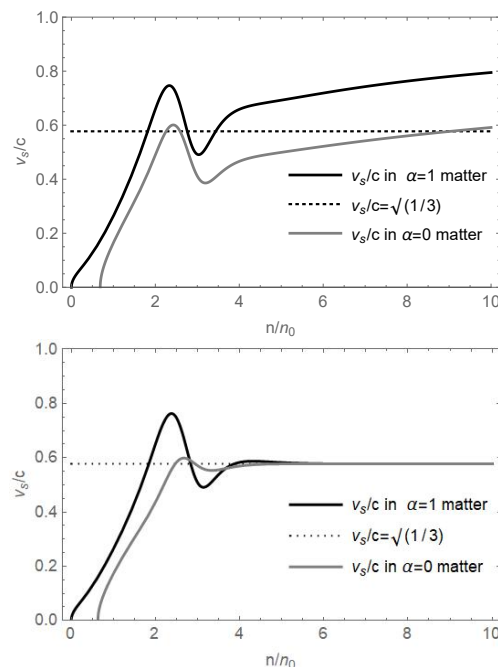
Figure 4. Sound velocity for $n_{\rm VM} = 6.75\, n_0$ (**upper panel**) and $20\, n_0$ (**lower panel**) for neutron matter ($\alpha = 1$) and symmetric matter ($\alpha = 0$), both computed in V_{lowk} RG with $n_{1/2} = 2.5\, n_0$ [77].

Let us focus on the scenario $C_0 \neq 0$, that is, where TEMT is a density-independent quantity. This scenario does feature in the chiral-scale EFT approach to nuclear matter. In the mean field approach it is shown that, going toward the DLFP, the TEMT $\langle \theta_\mu^\mu \rangle$ is a function of only the dilaton condensate [71]. In the skyrmion crystal approach to

nuclear matter it was found that the nucleon mass goes to a constant $\sim m_0$ after topology change due to the emergence of parity-doubling [42]. If this works in the mean field approach, $\langle \theta^\mu_\mu \rangle$ will be independent of density. This is indeed confirmed in the full V_{lowk} RG calculation, specifically for $n \gtrsim n_{1/2}$. In Figure 5, the TEMT (upper panel) is shown that gives the conformal velocity for $n \gtrsim 3\,n_0 > n_{1/2}$ (lower panel) using the scaling parameters discussed above.

One can easily see that the scenario $\langle \theta^\mu_\mu \rangle = C_0 \neq 0$ means that the sound velocity saturates the conformal limit but the conformal symmetry is not restored. We call this matter pseudoconformal matter, in which the nucleon has a constant effective mass and the pion decay constant is not zero.
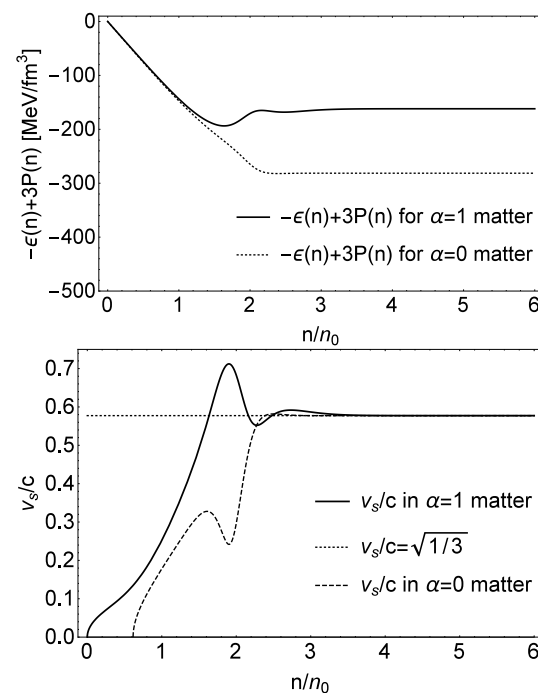
Figure 5. The density dependence of $\langle \theta^\mu_\mu \rangle$ (**upper panel**) and v_s (**lower panel**) for $\alpha = 0$ (nuclear matter) and $\alpha = 1$ (neutron matter) in V_{lowk} RG for $n_{1/2} = 2\,n_0$ and $n_{\rm VM} = 25\,n_0$ [5].

A recent analysis combining the astrophysical observations and model-independent theoretical ab initio calculations [116] shows that in the core of massive stars the sound velocity approaches the conformal limit $v_s^2/c^2 \to 1/3$ and the polytropic index takes the value $\gamma < 1.75$—a value close to the minimal one obtained in hadronic models. Therefore the core of massive stars is populated by "deconfined" quarks. An explicit calculation shows that the polytropic index $\gamma < 1.75$ in the PCM (see Figure 6), but we are still in the confined phase. Therefore the smallness of the polytropic index and conformal velocity cannot be regarded as sufficient criteria for the appearance of the deconfined quark.

Finally we compare our prediction for P/ϵ for $n_{1/2} = 2.5n_0$ with that obtained by the sound velocity interpolation method in Figure 7 [116]. We see that our prediction is not inside but parallel to the conformality band. The most significant point is that it lies above this band. The parallelism and location of our prediction come from the fact that in PCM the TEMT is positive and density-independent, as seen from the upper panel of Figure 5. It seems that, as a whole, the predictions of GnEFT resemble the "deconfined" quark structure [116]. However, there are intrinsic differences. First of all, in PCM, conformality is broken in the cores of massive stars. Most importantly, the half-skyrmion in PCM is still a colorless object. It is neither pure baryon with baryon number one nor purely quarkonic but a quasiparticle with fractional baryon charge. In fact it can be anyonic lying on a $(2+1)$ dimensional sheet [7].
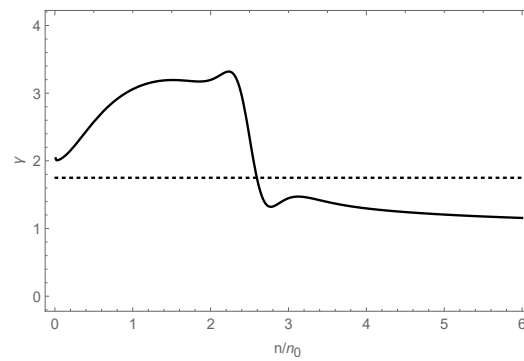
Figure 6. The polytropic index $\gamma = d\ln P / d\ln \epsilon$ as a function of density in neutron matter from the pseudo-conformal model with typical value $n_{1/2} = 2.5 n_0$ [14].
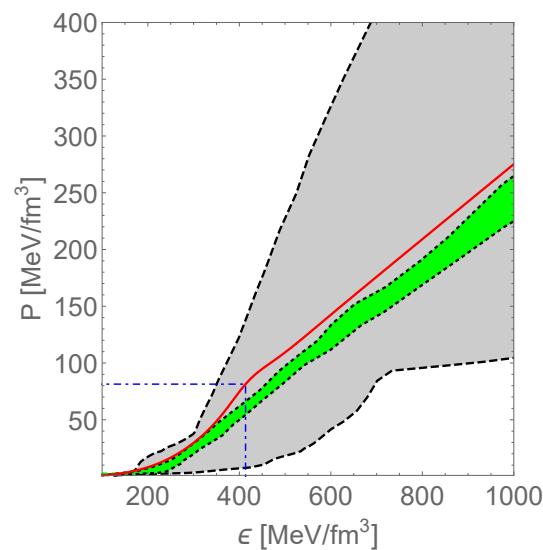

Figure 7. Comparison of (P/ϵ) between the PCM velocity (red line) and the band generated with the sound velocity interpolation method used in [116]. The location of the topology change is denoted by the dash-dotted line.

5.3. Equation of State

We next compute the equation of state of the pseudoconformal dense nuclear matter and compare it to the constraint from the astrophysical observation and gravitational wave detection. We also vary the last parameter in the model $n_{1/2}$ to see its effect on the EoS.

We should say that, whatever the topology change density $n_{1/2} \gtrsim 2n_0$ is, properties of the ordinary nuclear matter are fixed as stated already. In addition, we assume and actually numerically checked that for $n \gtrsim n_{1/2}$, slightly above that transition density, the sound velocity must be $v_s^2/c^2 \approx 1/3$.

It turns out that the energy per-particle E/A at $n \gtrsim n_{1/2}$ can be fitted by a two-parameter formula

$$E/A = -m_N + X^\alpha x^{1/3} + Y^\alpha x^{-1} \tag{53}$$

where X and Y are parameters to be fixed, $\alpha = (N-Z)/(N+Z)$, and $x \equiv n/n_0$. From (53), one concludes that the sound velocity satisfies

$$\frac{v_s^2}{c^2} = \frac{1}{3}, \tag{54}$$

independently of X^α and Y^α.

The full E/A from low to high density is obtained by uniting that given by V_{lowk} in R-I ($n < n_{1/2}$) and that given by Equation (53) in R-II ($n \geq n_{1/2}$). The parameters X^α and Y^α are fixed by the continuity at $n = n_{1/2}$ of the chemical potential and pressure

$$\mu_I = \mu_{II}, \; P_I = P_{II} \; \text{at} \; n = n_{1/2}. \tag{55}$$

We refer to such obtained EoS as the pseudoconformal model for compact star matter. It is found that this EoS works well for both pure ($\alpha = 1$) and symmetric ($\alpha = 0$) nuclear matter in the entire range of densities appropriate for massive compact stars, say up to $n \sim (6\text{–}7)n_0$ [10].

Note that the continuity (55) at $n = n_{1/2}$ follows from the fact that in the present approach there is no Ginzburg–Landau-type phase transition. The EoS with the first-order transition between the hadronic and the quark phases can be parameterized by using either the Gibbs construction [117,118] or Maxwell construction [119,120], which is not applicable in the present approach.

Since the energy density ϵ and pressure P relate to the energy per-particle (53) through

$$
\begin{aligned}
\epsilon &= n_0 x (m_N + E/A), \\
P &= n_0 x^2 \frac{d(E/A + m_N)}{dx},
\end{aligned}
\tag{56}
$$

we have

$$\langle \theta^\mu_\mu \rangle = \epsilon - 3P = 2n_0 Y^\alpha. \tag{57}$$

Therefore, the constant C_0 defined in Equation (52) is given by

$$C_0 = 2n_0 Y^\alpha. \tag{58}$$

Since Y^α is fixed by the continuity (55), C_0, the magnitude of the scale symmetry, is totally fixed by the nuclear properties in R-I which is constrained by that around saturation density.

We plot the sound velocity in Figure 8 by varying $n_{1/2}$. From this figure, one can easily see that after $n_{1/2}$, the conformal sound velocity $v_s^2/c^2 = 1/3$ emerges which indicates the emergence of pseudoconformal symmetry. It is clear from Figure 8 that the sound velocity for the case of $n_{1/2} = 4n_0$ violates the causality bound $v_s^2/c^2 < 1$. One may see that there is a spike around the location of the topology change. It may be an artifact of the sharp connection made at the boundary. What we want to emphasize, however, is that the rapid increase of the sound velocity at the transition point signals the changeover of the degrees of freedom [121] and the derivative contribution from the trace anomaly [28,29]. Significantly, this allows us to set the constraint for $n_{1/2}$

$$2\,n_0 \lesssim n_{1/2} \lesssim 4\,n_0. \tag{59}$$

What is important regarding this constraint is that the emergence of the conformal sound velocity which signals the precocious emergence of pseudo-conformality in compact stars is an order of magnitude lower than the asymptotic density $\gtrsim 50\,n_0$ predicted by perturbative QCD. By using the quarkyonic model, a recent detailed analysis of currently available data does confirm the onset density of $v_c^2 \approx 1/3$ at $\sim 4\,n_0$ [25–27].

We plot the predicted pressure P for $n_{1/2}/n_0 = 3, 4$ in comparision with the available heavy-ion data [122] in Figure 9. It should be noted that although the predicted pressure for $n_{1/2} = 4n_0$ is consistent with the bound at $n \sim 6n_0$, it is beyond the available experimental bound at $n \sim 4n_0$. Although this may again be an artifact of the sharp matching, it puts $n_{1/2} \simeq 4n_0$ in tension with nature. Nonetheless it may be too hasty to rule out the threshold density $n_{1/2} = 4n_0$.
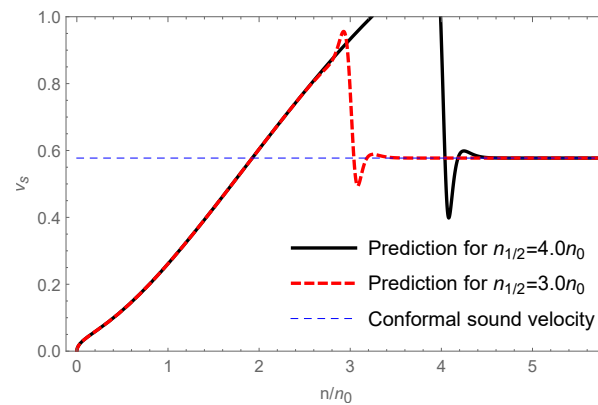
Figure 8. Density dependence of the sound velocity in neutron matter with different $n_{1/2}$ [5].
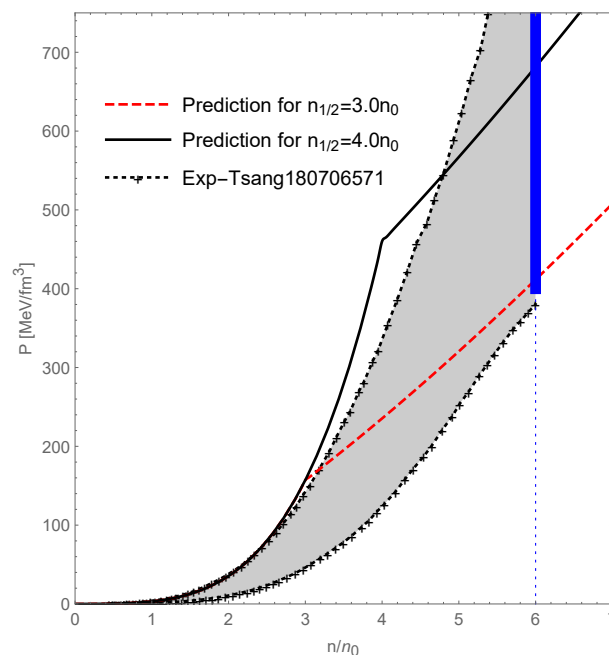

Figure 9. Comparision of the density dependence of the pressure for neutron matter ($\alpha = 1$) with the available experimental bound (shaded) given in [122]. The bound at $6n_0$ is indicated by the blue band.

6. Star Properties and Gravitational Waves

The final topic we want to discuss in this review is the confrontation of the PCM with star properties and gravitational wave detection with the purpose of showing the rationality of the PCM.

Duly taking the pressures of leptons in beta equilibrium into account, the solution of the TOV equation yields the results for the mass-radius relation of a neutron star. It has been found that the maximum mass of a neutron star in the PCM is roughly $2.04M_\odot \sim 2.23M_\odot$ for $2.0 \leq n_{1/2}/n_0 \leq 4.0$ which is consistent with the present astrophysical observation [123–125]. We plot the M-R relation with the typical value $n_{1/2} = 2.5\, n_0$ in Figure 10. One can easily see that the present calculation is consistent with the observations.

Next, let us turn to how our theory fares with what came out of the LIGO/Virgo gravitational observations. The quantities that we will consider are the dimensionless tidal deformability Λ_i for the star M_i and $\tilde{\Lambda}$ defined by

$$\tilde{\Lambda} = \frac{16}{13} \frac{(M_1 + 12M_2)M_1^4\Lambda_1 + (M_2 + 12M_1)M_2^4\Lambda_2}{(M_1 + M_2)^5} \tag{60}$$

for M_1 and M_2 constrained to the well-measured "chirp mass"

$$\mathcal{M} = \frac{(M_1 M_2)^{3/5}}{(M_1 + M_2)^{1/5}} = 1.188 M_\odot. \tag{61}$$

To confront the LIGO/Virgo data, we plot our prediction for Λ_1 vs. Λ_2 in Figure 11. As it stands, our prediction is compatible with the LIGO/Virgo constraint for $n_{1/2} \gtrsim 2\,n_0$. Although there seems to be some tensions with the pressure, the result for $n_{1/2} = 4\,n_0$ is of a quality comparable to that of $n_{1/2} = 3\,n_0$.
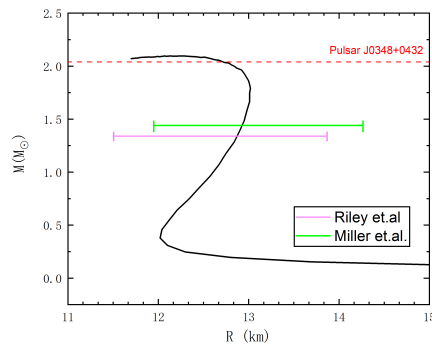
Figure 10. M-R relation from PCM with observed mass of pulsar J0348 + 0432 [124] and radius constraints [126,127] from NICER [77].
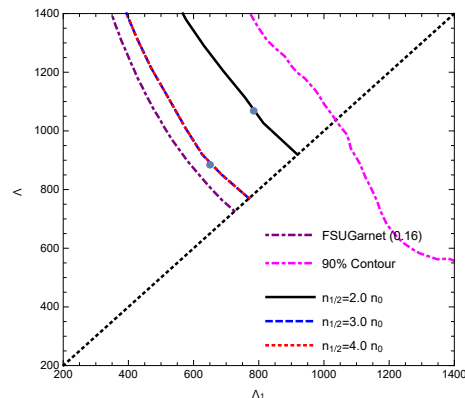
Figure 11. Tidal deformabilities Λ_1 and Λ_2 of the components of the binary neutron star system GW170817 with chirp mass $1.188 M_\odot$ [5]. The constraint from GW170817 at the 90% probability contour and the result from "FSUGarnet (0.16)" [128] are also quoted for reference.

7. Summary and Perspective

We reviewed in this work the possible emergent symmetries and topology change in dense compact star matter. The information of the medium-modified hadron properties obtained from the skyrmion crystal approach, in addition to the presumed emergent scale and local flavor symmetries, inspired the construction of the pseudoconformal model of dense compact star matter.

In the pseudoconformal model, a peculiar feature that has not been observed by any other models before is that, in compact star matter, the trace of the energy-momentum tensor is a nonzero, density-independent quantity and therefore, induces the precious appearance of the conformal sound velocity $v_s^2/c^2 = 1/3$, in stark contrast to what has been widely accepted in society [20]. That is, there is a pseudoconformal symmetry in the compact star matter. The predictions of the pseudoconformal model are consistent with all the constraints from all the terrestrial experiments and astrophysical observations.

In the present approach, the peudoconformal model is made of a quasiparticle with fractional baryon charge, such as an anyon. Actually, in the literature, not only the con-

stituents of the compact star matter at $n \gtrsim 2n_0$ are under debate, but the state of the matter is also not well understood. The state of a compact star could be, for example, a Fermi-liquid [129], a non-Fermi-liquid [130], a (2 + 1)-dimensional sheet [7], a crystal lattice made of baryonic popcorn [131], and so on. It is interesting to explore the diagnosis of these possibilities.

We finally devote ourselves to the possible extensions and revisions of the model.

The idea of the chiral-scale EFT à la Crewther and Tunstall ,which GnEFT is based on, is anchored on three-flavor QCD. Therefore $f_0(500)$ can be taken as the same footing as the pseudoscalar mesons pion and kaon. However, in the present approach, we only included the up and down quarks and ignored the strange degrees of freedom for simplicity. It is therefore interesting to extend the present framework to see the effect of strangeness on compact star matter [132]. In addition, it is also interesting to extend the present approach to include the Δ baryons and hyperons [133–135].

Another issue that should be considered in extensions of the present work is to include the corrections to the presently applied LOSS. With these corrections, not only the hadron masses, but also the coupling constants have IDD. Therefore, both the stiffness of the EoS and the tidal deformability of the compact star may be changed. In addition, due to these corrections which explicitly violate the conformal symmetry, the sound velocity after the topology change may deviate from the conformal limit. It should be noted that, since the correction from the explicit breaking of the conformal limit is taken as a perturbative one, the global picture of the compact star discussed is intact.

Finally, it is interesting to pin down the location at which the hidden scale and local flavor symmetries are restored. As we explicitly discussed above, this is encoded in the IDDs of the hadron parameters such as the pion decay constant, dilaton decay constant, rho-N-N coupling and rho meson mass. By checking the location dependence of the star properties as well the waveforms of the gravitational waves, one can also extract information on the emergent symmetries and consequently the phase structure of QCD at low temperature [136] since the gravitational waves emitted from the binary neutron star merger carry the information of the equation of state of the nuclear matter [137–140].

Author Contributions: Both authors contributed equally to the review. All authors have read and agreed to the published version of the manuscript.

References

1. Brown, G.E.; Rho, M. On the manifestation of chiral symmetry in nuclei and dense nuclear matter. *Phys. Rep.* **2002**, *363*, 85–171. [CrossRef]
2. Holt, J.W.; Rho, M.; Weise, W. Chiral symmetry and effective field theories for hadronic, nuclear and stellar matter. *Phys. Rept.* **2016**, *621*, 2–75. [CrossRef]
3. Drews, M.; Weise, W. Functional renormalization group studies of nuclear and neutron matter. *Prog. Part. Nucl. Phys.* **2017**, *93*, 69–107. [CrossRef]
4. Baym, G.; Hatsuda, T.; Kojo, T.; Powell, P.D.; Song, Y.; Takatsuka, T. From hadrons to quarks in neutron stars: A review. *Rep. Prog. Phys.* **2018**, *81*, 056902. [CrossRef]
5. Ma, Y.L.; Rho, M. Towards the hadron–quark continuity via a topology change in compact stars. *Prog. Part. Nucl. Phys.* **2020**, *113*, 103791. [CrossRef]

6. Li, B.A.; Krastev, P.G.; Wen, D.H.; Zhang, N.B. Towards Understanding Astrophysical Effects of Nuclear Symmetry Energy. *Eur. Phys. J. A* **2019**, *55*, 117. [CrossRef]

7. Ma, Y.L.; Rho, M. Dichotomy of Baryons as Quantum Hall Droplets and Skyrmions: Topological Structure of Dense Matter. *Symmetry* **2021**, *13*, 1888. [CrossRef]

8. Lovato, A.; Dore, T.; Pisarski, R.D.; Schenke, B.; Chatziioannou, K.; Read, J.S.; Landry, P.; Danielewicz, P.; Lee, D.; Pratt, S.; et al. Long Range Plan: Dense matter theory for heavy-ion collisions and neutron stars. *arXiv* **2022**, arXiv:2211.02224.

9. Paeng, W.G.; Kuo, T.T.S.; Lee, H.K.; Rho, M. Scale-Invariant Hidden Local Symmetry, Topology Change and Dense Baryonic Matter. *Phys. Rev. C* **2016**, *93*, 055203. [CrossRef]

10. Paeng, W.G.; Kuo, T.T.S.; Lee, H.K.; Ma, Y.L.; Rho, M. Scale-invariant hidden local symmetry, topology change, and dense baryonic matter. II. *Phys. Rev. D* **2017**, *96*, 014031. [CrossRef]

11. Ma, Y.L.; Lee, H.K.; Paeng, W.G.; Rho, M. Pseudoconformal equation of state in compact-star matter from topology change and hidden symmetries of QCD. *Sci. China Phys. Mech. Astron.* **2019**, *62*, 112011. [CrossRef]

12. Ma, Y.L.; Rho, M. Pseudoconformal structure in dense baryonic matter. *Phys. Rev. D* **2019**, *99*, 014034. [CrossRef]

13. Ma, Y.L.; Rho, M. Sound velocity and tidal deformability in compact stars. *Phys. Rev. D* **2019**, *100*, 114003. [CrossRef]

14. Ma, Y.L.; Rho, M. What's in the core of massive neutron stars? *arXiv* **2020**, arXiv:2006.14173.

15. Rho, M.; Ma, Y.L. Manifestation of Hidden Symmetries in Baryonic Matter: From Finite Nuclei to Neutron Stars. *Mod. Phys. Lett. A* **2021**, *36*, 2130012. [CrossRef]

16. Ma, Y.L.; Rho, M. Topology change, emergent symmetries and compact star matter. *AAPPS Bull.* **2021**, *31*, 16. [CrossRef]

17. Lee, H.K.; Ma, Y.L.; Paeng, W.G.; Rho, M. Cusp in the symmetry energy, speed of sound in neutron stars and emergent pseudo-conformal symmetry. *Mod. Phys. Lett. A* **2022**, *37*, 2230003. [CrossRef]

18. Rho, M. Mapping Topology of Skyrmions and Fractional Quantum Hall Droplets to Nuclear EFT for Ultra-Dense Baryonic Matter. *Symmetry* **2022**, *14*, 994. [CrossRef]

19. Bedaque, P.; Steiner, A.W. Sound velocity bound and neutron stars. *Phys. Rev. Lett.* **2015**, *114*, 031103. [CrossRef]

20. Tews, I.; Carlson, J.; Gandolfi, S.; Reddy, S. Constraining the speed of sound inside neutron stars with chiral effective field theory interactions and observations. *Astrophys. J.* **2018**, *860*, 149. [CrossRef]

21. Moustakidis, C.C.; Gaitanos, T.; Margaritis, C.; Lalazissis, G.A. Bounds on the speed of sound in dense matter, and neutron star structure. *Phys. Rev. C* **2017**, *95*, 045801; Erratum: *Phys. Rev. C* **2017**, *95*, 059904. [CrossRef]

22. Alsing, J.; Silva, H.O.; Berti, E. Evidence for a maximum mass cut-off in the neutron star mass distribution and constraints on the equation of state. *Mon. Not. R. Astron. Soc.* **2018**, *478*, 1377–1391. [CrossRef]

23. McLerran, L.; Reddy, S. Quarkyonic Matter and Neutron Stars. *Phys. Rev. Lett.* **2019**, *122*, 122701. [CrossRef] [PubMed]

24. Jeong, K.S.; McLerran, L.; Sen, S. Dynamically generated momentum space shell structure of quarkyonic matter via an excluded volume model. *Phys. Rev. C* **2020**, *101*, 035201. [CrossRef]

25. Kapusta, J.I.; Welle, T. Neutron stars with a crossover equation of state. *Phys. Rev. C* **2021**, *104*, L012801. [CrossRef]

26. Zhao, T.; Lattimer, J.M. Quarkyonic Matter Equation of State in Beta-Equilibrium. *Phys. Rev. D* **2020**, *102*, 023021. [CrossRef]

27. Margueron, J.; Hansen, H.; Proust, P.; Chanfray, G. Quarkyonic stars with isospin-flavor asymmetry. *Phys. Rev. C* **2021**, *104*, 055803. [CrossRef]

28. Fujimoto, Y.; Fukushima, K.; McLerran, L.D.; Praszalowicz, M. Trace anomaly as signature of conformality in neutron stars. *Phys. Rev. Lett.* **2022**, *129*, 252702. [CrossRef]

29. Marczenko, M.; McLerran, L.; Redlich, K.; Sasaki, C. Reaching percolation and conformal limits in neutron stars. *Phys. Rev. C* **2022**, *107*, 025802. [CrossRef]

30. Bando, M.; Kugo, T.; Uehara, S.; Yamawaki, K.; Yanagida, T. Is rho Meson a Dynamical Gauge Boson of Hidden Local Symmetry? *Phys. Rev. Lett.* **1985**, *54*, 1215. [CrossRef]

31. Bando, M.; Kugo, T.; Yamawaki, K. Nonlinear Realization and Hidden Local Symmetries. *Phys. Rep.* **1988**, *164*, 217–314. [CrossRef]

32. Harada, M.; Yamawaki, K. Hidden local symmetry at loop: A New perspective of composite gauge boson and chiral phase transition. *Phys. Rep.* **2003**, *381*, 1–233. [CrossRef]

33. Crewther, R.J.; Tunstall, L.C. $\Delta I = 1/2$ rule for kaon decays derived from QCD infrared fixed point. *Phys. Rev. D* **2015**, *91*, 034016. [CrossRef]

34. Catà, O.; Crewther, R.J.; Tunstall, L.C. Crawling technicolor. *Phys. Rev. D* **2019**, *100*, 095007. [CrossRef]

35. Crewther, R.J. Genuine Dilatons in Gauge Theories. *Universe* **2020**, *6*, 96. [CrossRef]

36. Skyrme, T.H.R. A Nonlinear field theory. *Proc. R. Soc. Lond. A* **1961**, *260*, 127–138. [CrossRef]

37. Kugler, M.; Shtrikman, S. A New Skyrmion Crystal. *Phys. Lett. B* **1988**, *208*, 491–494. [CrossRef]

38. Kugler, M.; Shtrikman, S. Skyrmion Crystals and Their Symmetries. *Phys. Rev. D* **1989**, *40*, 3421. [CrossRef] [PubMed]

39. Lee, H.J.; Park, B.Y.; Rho, M.; Vento, V. Sliding vacua in dense skyrmion matter. *Nucl. Phys. A* **2003**, *726*, 69–92. [CrossRef]

40. Park, B.Y.; Rho, M.; Vento, V. Vector mesons and dense Skyrmion matter. *Nucl. Phys. A* **2004**, *736*, 129–145. [CrossRef]

41. Park, B.Y.; Rho, M.; Vento, V. The Role of the Dilaton in Dense Skyrmion Matter. *Nucl. Phys. A* **2008**, *807*, 28–37. [CrossRef]

42. Ma, Y.L.; Harada, M.; Lee, H.K.; Oh, Y.; Park, B.Y.; Rho, M. Dense baryonic matter in the hidden local symmetry approach: Half-skyrmions and nucleon mass. *Phys. Rev. D* **2013**, *88*, 014016; Erratum: *Phys. Rev. D* **2013**, *88*, 079904. [CrossRef]

43. Ma, Y.L.; Harada, M.; Lee, H.K.; Oh, Y.; Park, B.Y.; Rho, M. Dense baryonic matter in conformally-compensated hidden local symmetry: Vector manifestation and chiral symmetry restoration. *Phys. Rev. D* **2014**, *90*, 034015. [CrossRef]

44. Ma, Y.L.; Rho, M. Recent progress on dense nuclear matter in skyrmion approaches. *Sci. China Phys. Mech. Astron.* **2017**, *60*, 032001. [CrossRef]

45. Shao, L.Q.; Ma, Y.L. Scale symmetry and composition of compact star matter. *Phys. Rev. D* **2022**, *106*, 014014. [CrossRef]

46. Brown, G.E.; Rho, M. Scaling effective Lagrangians in a dense medium. *Phys. Rev. Lett.* **1991**, *66*, 2720–2723. [CrossRef] [PubMed]

47. Bogner, S.K.; Kuo, T.T.S.; Schwenk, A.; Entem, D.R.; Machleidt, R. Towards a model independent low momentum nucleon nucleon interaction. *Phys. Lett. B* **2003**, *576*, 265–272. [CrossRef]

48. Bogner, S.K.; Schwenk, A.; Kuo, T.T.S.; Brown, G.E. Renormalization group equation for low momentum effective nuclear interactions. *arXiv* **2001**, arXiv:nucl-th/0111042.

49. Bogner, S.K.; Kuo, T.T.S.; Schwenk, A. Model independent low momentum nucleon interaction from phase shift equivalence. *Phys. Rep.* **2003**, *386*, 1–27. [CrossRef]

50. Serot, B.D.; Walecka, J.D. The Relativistic Nuclear Many Body Problem. *Adv. Nucl. Phys.* **1986**, *16*, 1–327.

51. Li, F.; Cai, B.J.; Zhou, Y.; Jiang, W.Z.; Chen, L.W. Effects of Isoscalar- and Isovector-scalar Meson Mixing on Neutron Star Structure. *Astrophys. J.* **2022**, *929*, 183. [CrossRef]

52. Miyatsu, T.; Cheoun, M.K.; Saito, K. Asymmetric Nuclear Matter in Relativistic Mean-field Models with Isoscalar- and Isovector-meson Mixing. *Astrophys. J.* **2022**, *929*, 82. [CrossRef]

53. Workman, R.L. Review of Particle Physics. *Prog. Theor. Exp. Phys.* **2022**, *2022*, 083C01. [CrossRef]

54. Isham, C.J.; Salam, A.; Strathdee, J.A. Broken chiral and conformal symmetry in an effective-lagrangian formalism. *Phys. Rev. D* **1970**, *2*, 685–690. [CrossRef]

55. Ellis, J.R. Aspects of conformal symmetry and chirality. *Nucl. Phys. B* **1970**, *22*, 478–492; Erratum: *Nucl. Phys. B* **1971**, *25*, 639. [CrossRef]

56. Schechter, J. Effective Lagrangian with Two Color Singlet Gluon Fields. *Phys. Rev. D* **1980**, *21*, 3393–3400. [CrossRef]

57. Golterman, M.; Shamir, Y. Low-energy effective action for pions and a dilatonic meson. *Phys. Rev. D* **2016**, *94*, 054502. [CrossRef]

58. Brodsky, S.J.; de Teramond, G.F.; Deur, A. Nonperturbative QCD Coupling and its β-function from Light-Front Holography. *Phys. Rev. D* **2010**, *81*, 096010. [CrossRef]

59. Horsley, R.; Perlt, H.; Rakow, P.E.L.; Schierholz, G.; Schiller, A. The SU(3) Beta Function from Numerical Stochastic Perturbation Theory. *Phys. Lett. B* **2014**, *728*, 1–4. [CrossRef]

60. Yu, Q.; Zhou, H.; Huang, X.D.; Shen, J.M.; Wu, X.G. Novel and Self-Consistency Analysis of the QCD Running Coupling α_s(Q) in Both the Perturbative and Nonperturbative Domains. *Chin. Phys. Lett.* **2022**, *39*, 071201. [CrossRef]

61. Alexandru, A.; Horváth, I. Possible New Phase of Thermal QCD. *Phys. Rev. D* **2019**, *100*, 094507. [CrossRef]

62. Freund, P.G.O.; Nambu, Y. Scalar field coupled to the trace of the energy-momentum tensor. *Phys. Rev.* **1968**, *174*, 1741–1743. [CrossRef]

63. Fubini, S. A New Approach to Conformal Invariant Field Theories. *Nuovo Cim. A* **1976**, *34*, 521. [CrossRef]

64. Serra, J. A higgs-like dilaton: Viability and implications. *EPJ Web Conf.* **2013**, *60*, 17005. [CrossRef]

65. Goldberger, W.D.; Grinstein, B.; Skiba, W. Distinguishing the Higgs boson from the dilaton at the Large Hadron Collider. *Phys. Rev. Lett.* **2008**, *100*, 111802. [CrossRef]

66. Li, Y.L.; Ma, Y.L.; Rho, M. Chiral-scale effective theory including a dilatonic meson. *Phys. Rev. D* **2017**, *95*, 114011. [CrossRef]

67. Catà, O.; Müller, C. Chiral effective theories with a light scalar at one loop. *Nucl. Phys. B* **2020**, *952*, 114938. [CrossRef]

68. Li, Y.L.; Ma, Y.L.; Rho, M. Nuclear Axial Currents from Scale-Chiral Effective Field Theory. *Chin. Phys. C* **2018**, *42*, 094102. [CrossRef]

69. Li, Y.L.; Ma, Y.L.; Rho, M. Nonquenching of g_A in nuclei, Landau-Migdal fixed-point theory, and emergence of scale symmetry in dense baryonic matter. *Phys. Rev. C* **2018**, *98*, 044318. [CrossRef]

70. Ma, Y.L.; Rho, M. Quenched g_A in Nuclei and Emergent Scale Symmetry in Baryonic Matter. *Phys. Rev. Lett.* **2020**, *125*, 142501. [CrossRef]

71. Paeng, W.G.; Lee, H.K.; Rho, M.; Sasaki, C. Dilaton-Limit Fixed Point in Hidden Local Symmetric Parity Doubled Model. *Phys. Rev. D* **2012**, *85*, 054022. [CrossRef]

72. Georgi, H. New Realization of Chiral Symmetry. *Phys. Rev. Lett.* **1989**, *63*, 1917–1919. [CrossRef] [PubMed]

73. Georgi, H. Vector Realization of Chiral Symmetry. *Nucl. Phys. B* **1990**, *331*, 311–330. [CrossRef]

74. Harada, M.; Yamawaki, K. Vector manifestation of the chiral symmetry. *Phys. Rev. Lett.* **2001**, *86*, 757–760. [CrossRef] [PubMed]

75. Beane, S.R.; van Kolck, U. The Dilated chiral quark model. *Phys. Lett. B* **1994**, *328*, 137–142. [CrossRef]

76. Suzuki, M. Inevitable emergence of composite gauge bosons. *Phys. Rev. D* **2017**, *96*, 065010. [CrossRef]

77. Yang, W.C.; Ma, Y.L. Vector manifestation, conformality and sound velocity in compact star matter. In manuscript in preparation.

78. Witten, E. Baryons in the 1/n Expansion. *Nucl. Phys. B* **1979**, *160*, 57–115. [CrossRef]

79. Brown, G.E.; Rho, M. (Eds.) *The Multifaceted Skyrmion*; World Scientific: Singapore, 2010. [CrossRef]

80. Manton, N.S. *Skyrmions—A Theory of Nuclei*; World Scientific: Singapore, 2022. [CrossRef]

81. Klebanov, I.R. Nuclear Matter in the Skyrme Model. *Nucl. Phys. B* **1985**, *262*, 133–143. [CrossRef]

82. Goldhaber, A.S.; Manton, N.S. Maximal Symmetry of the Skyrme Crystal. *Phys. Lett. B* **1987**, *198*, 231–234. [CrossRef]

83. Ma, Y.L.; Harada, M. Lecture notes on the Skyrme model. *arXiv* **2016**, arXiv:1604.04850.

84. Ma, Y.L.; Harada, M.; Lee, H.K.; Oh, Y.; Rho, M. Skyrmions, half-skyrmions and nucleon mass in dense baryonic matter. *Int. J. Mod. Phys. Conf. Ser.* **2014**, *29*, 1460238. [CrossRef]

85. Harada, M.; Lee, H.K.; Ma, Y.L.; Rho, M. Inhomogeneous quark condensate in compressed Skyrmion matter. *Phys. Rev. D* **2015**, *91*, 096011. [CrossRef]

86. Detar, C.E.; Kunihiro, T. Linear σ Model with Parity Doubling. *Phys. Rev. D* **1989**, *39*, 2805. [CrossRef] [PubMed]

87. Motohiro, Y.; Kim, Y.; Harada, M. Asymmetric nuclear matter in a parity doublet model with hidden local symmetry. *Phys. Rev. C* **2015**, *92*, 025201; Erratum: *Phys. Rev. C* **2017**, *95*, 059903. [CrossRef]

88. Komargodski, Z. Baryons as Quantum Hall Droplets. *arXiv* **2018**, arXiv:1812.09253.

89. Hsin, P.S.; Seiberg, N. Level/rank Duality and Chern-Simons-Matter Theories. *J. High Energy Phys.* **2016**, *9*, 95. [CrossRef]

90. Gaiotto, D.; Komargodski, Z.; Seiberg, N. Time-reversal breaking in QCD$_4$, walls, and dualities in 2 + 1 dimensions. *J. High Energy Phys.* **2018**, *1*, 110. [CrossRef]

91. Benini, F. Three-dimensional dualities with bosons and fermions. *J. High Energy Phys.* **2018**, *2*, 68. [CrossRef]

92. Tong, D. Lectures on the Quantum Hall Effect. *arXiv* **2016**, arXiv:1606.06687.

93. Karasik, A. Skyrmions, Quantum Hall Droplets, and one current to rule them all. *SciPost Phys.* **2020**, *9*, 8. [CrossRef]

94. Bigazzi, F.; Cotrone, A.L.; Olzi, A. Hall Droplet Sheets in Holographic QCD. *J. High Energ. Phys.* **2023**, *194*. [CrossRef]

95. Liu, X.H.; Ma, Y.L.; Rho, M. Topology change and nuclear symmetry energy in compact-star matter. *Phys. Rev. C* **2019**, *99*, 055808. [CrossRef]

96. Ma, Y.L.; Nowak, M.A.; Rho, M.; Zahed, I. Baryon as a Quantum Hall Droplet and the Cheshire Cat Principle. *Phys. Rev. Lett.* **2019**, *123*, 172301. [CrossRef] [PubMed]

97. Callan, C.G., Jr.; Harvey, J.A. Anomalies and Fermion Zero Modes on Strings and Domain Walls. *Nucl. Phys. B* **1985**, *250*, 427–436. [CrossRef]

98. Pisarski, R.D.; Wilczek, F. Remarks on the Chiral Phase Transition in Chromodynamics. *Phys. Rev. D* **1984**, *29*, 338–341. [CrossRef]

99. Park, B.Y.; Paeng, W.G.; Vento, V. The Inhomogeneous Phase of Dense Skyrmion Matter. *Nucl. Phys. A* **2019**, *989*, 231–245. [CrossRef]

100. Canfora, F. Ordered arrays of Baryonic tubes in the Skyrme model in (3 + 1) dimensions at finite density. *Eur. Phys. J. C* **2018**, *78*, 929. [CrossRef]

101. Rho, M. Probing Fractional Quantum Hall Sheets in Dense Baryonic Matter. *arXiv* **2022**, arXiv:2211.14890.

102. Sulejmanpasic, T.; Shao, H.; Sandvik, A.; Unsal, M. Confinement in the bulk, deconfinement on the wall: Infrared equivalence between compactified QCD and quantum magnets. *Phys. Rev. Lett.* **2017**, *119*, 091601. [CrossRef]

103. Senthil, T.; Vishwanath, A.; Balents, L.; Sachdev, S.; Fisher, M.P.A. Deconfined Quantum Critical Points. *Science* **2004**, *303*, 1490–1494. [CrossRef] [PubMed]

104. Li, Y.L.; Ma, Y.L. Derivation of Brown–Rho Scaling from Scale-Chiral Perturbation Theory. 2017. Available online: https://arxiv.org/abs/1710.02839 (accessed on 6 February 2023).

105. Ma, Y.L.; Rho, M. Scale-chiral symmetry, ω meson and dense baryonic matter. *Phys. Rev. D* **2018**, *97*, 094017. [CrossRef]

106. Wilkinson, D.H. Renormalization of the Axial-Vector Coupling Constant in Nuclear beta Decay. *Phys. Rev. C* **1973**, *7*, 930–936. [CrossRef]

107. Suhonen, J.T. Value of the Axial-Vector Coupling Strength in β and $\beta\beta$ Decays: A Review. *Front. Phys.* **2017**, *5*, 55. [CrossRef]

108. Engel, J.; Menéndez, J. Status and Future of Nuclear Matrix Elements for Neutrinoless Double-Beta Decay: A Review. *Rep. Prog. Phys.* **2017**, *80*, 046301. [CrossRef] [PubMed]

109. Rho, M. How and How Much is g_A \it Fundamentally Quenched in Nuclei? *arXiv* **2022**, arXiv:2212.05558.

110. Friman, B.; Rho, M. From chiral Lagrangians to Landau Fermi liquid theory of nuclear matter. *Nucl. Phys. A* **1996**, *606*, 303–319. A [CrossRef]

111. Kienle, P.; Yamazaki, T. Pions in nuclei, a probe of chiral symmetry restoration. *Prog. Pa. Nucl. Phys.* **2004**, *52*, 85–132. [CrossRef]

112. Lubos, D.; Park, J.; Faestermann, T.; Gernhäuser, R.; Kruecken, R.; Lewitowicz, M.; Nishimura, S.; Sakurai, H.; Ahn, D.S.; Baba, H.; et al. Improved Value for the Gamow-Teller Strength of the ^{100}Sn Beta Decay. *Phys. Rev. Lett.* **2019**, *122*, 222502. [CrossRef]

113. van Kolck, U. Nuclear physics with an effective field theory around the unitarity limit. *Nuovo Cim. C* **2019**, *42*, 52. [CrossRef]

114. Tews, I.; Lattimer, J.M.; Ohnishi, A.; Kolomeitsev, E.E. Symmetry Parameter Constraints from a Lower Bound on Neutron-matter Energy. *Astrophys. J.* **2017**, *848*, 105. [CrossRef]

115. Dong, H.; Kuo, T.T.S.; Lee, H.K.; Machleidt, R.; Rho, M. Half-Skyrmions and the Equation of State for Compact-Star Matter. *Phys. Rev. C* **2013**, *87*, 054332. [CrossRef]

116. Annala, E.; Gorda, T.; Kurkela, A.; Nättilä, J.; Vuorinen, A. Evidence for quark-matter cores in massive neutron stars. *Nat. Phys.* **2020**, *16*, 907–910. [CrossRef]

117. Glendenning, N.K. First order phase transitions with more than one conserved charge: Consequences for neutron stars. *Phys. Rev. D* **1992**, *46*, 1274–1287. [CrossRef] [PubMed]

118. Macher, J.; Schaffner-Bielich, J. Phase transitions in compact stars. *Eur. J. Phys.* **2005**, *26*, 341–360. [CrossRef]

119. Alford, M.G.; Han, S.; Prakash, M. Generic conditions for stable hybrid stars. *Phys. Rev. D* **2013**, *88*, 083013. [CrossRef]

120. Han, S.; Steiner, A.W. Tidal deformability with sharp phase transitions in (binary) neutron stars. *Phys. Rev. D* **2019**, *99*, 083014. [CrossRef]

121. Hippert, M.; Fraga, E.S.; Noronha, J. Insights on the peak in the speed of sound of ultradense matter. *Phys. Rev. D* **2021**, *104*, 034011. [CrossRef]

122. Tsang, C.Y.; Tsang, M.B.; Danielewicz, P.; Lynch, W.G.; Fattoyev, F.J. Constraining neutron-star equation of state using heavy-ion collisions. *arXiv* **2018**, arXiv:1807.06571.

123. Demorest, P.; Pennucci, T.; Ransom, S.; Roberts, M.; Hessels, J. Shapiro Delay Measurement of a Two Solar Mass Neutron Star. *Nature* **2010**, *467*, 1081–1083. [CrossRef]

124. Antoniadis, J.; Freire, P.C.; Wex, N.; Tauris, T.M.; Lynch, R.S.; Van Kerkwijk, M.H.; Kramer, M.; Bassa, C.; Dhillon, V.S.; Driebe, T.; et al. A Massive Pulsar in a Compact Relativistic Binary. *Science* **2013**, *340*, 6131. [CrossRef] [PubMed]

125. Cromartie, H.T.; Fonseca, E.; Ransom, S.M.; Demorest, P.B.; Arzoumanian, Z.; Blumer, H.; Brook, P.R.; DeCesar, M.E.; Dolch, T.; Ellis, J.A.; et al. Relativistic Shapiro delay measurements of an extremely massive millisecond pulsar. *Nature Astron.* **2019**, *4*, 72–76. [CrossRef]

126. Raaijmakers, G.; Riley, T.E.; Watts, A.L.; Greif, S.K.; Morsink, S.M.; Hebeler, K.; Schwenk, A.; Hinderer, T.; Nissanke, S.; Guillot, S.; et al. A *NICER* view of PSR J0030+0451: Implications for the dense matter equation of state. *Astrophys. J. Lett.* **2019**, *887*, L22. [CrossRef]

127. Miller, M.C.; Lamb, F.K.; Dittmann, A.J.; Bogdanov, S.; Arzoumanian, Z.; Gendreau, K.C.; Guillot, S.; Harding, A.K.; Ho, W.C.G.; Lattimer, J.M.; et al. PSR J0030+0451 Mass and Radius from *NICER* Data and Implications for the Properties of Neutron Star Matter. *Astrophys. J. Lett.* **2019**, *887*, L24. [CrossRef]

128. Fattoyev, F.J.; Piekarewicz, J.; Horowitz, C.J. Neutron Skins and Neutron Stars in the Multimessenger Era. *Phys. Rev. Lett.* **2018**, *120*, 172702. [CrossRef]

129. Shankar, R. Renormalization group approach to interacting fermions. *Rev. Mod. Phys.* **1994**, *66*, 129–192. [CrossRef]

130. Lee, H.K.; Rho, M. Topology Change and Tensor Forces for the EoS of Dense Baryonic Matter. *Eur. Phys. J. A* **2014**, *50*, 14. [CrossRef]

131. Kaplunovsky, V.; Melnikov, D.; Sonnenschein, J. Baryonic Popcorn. *J. High Energy Phys.* **2012**, *11*, 47. [CrossRef]

132. Weise, W. Dense Baryonic Matter and Strangeness in Neutron Stars. *JPS Conf. Proc.* **2019**, *26*, 011002. [CrossRef]

133. Takeda, Y.; Kim, Y.; Harada, M. Catalysis of partial chiral symmetry restoration by Δ matter. *Phys. Rev. C* **2018**, *97*, 065202. [CrossRef]

134. Marczenko, M.; Redlich, K.; Sasaki, C. Reconciling Multi-messenger Constraints with Chiral Symmetry Restoration. *Astrophys. J. Lett.* **2022**, *925*, L23. [CrossRef]

135. Sedrakian, A.; Li, J.J.; Weber, F. Heavy Baryons in Compact Stars. *arXiv* **2022**, arXiv:2212.01086.

136. Yang, W.C.; Ma, Y.L.; Wu, Y.L. Topology change and emergent scale symmetry in compact star matter via gravitational wave detection. *Sci. China Phys. Mech. Astron.* **2021**, *64*, 252011. [CrossRef]

137. Hotokezaka, K.; Kyutoku, K.; Shibata, M. Exploring tidal effects of coalescing binary neutron stars in numerical relativity. *Phys. Rev. D* **2013**, *87*, 044001. [CrossRef]

138. Hotokezaka, K.; Kyutoku, K.; Okawa, H.; Shibata, M.; Kiuchi, K. Binary Neutron Star Mergers: Dependence on the Nuclear Equation of State. *Phys. Rev. D* **2011**, *83*, 124008. [CrossRef]

139. Bauswein, A.; Stergioulas, N. Unified picture of the post-merger dynamics and gravitational wave emission in neutron star mergers. *Phys. Rev. D* **2015**, *91*, 124056. [CrossRef]

140. Fujimoto, Y.; Fukushima, K.; Hotokezaka, K.; Kyutoku, K. Gravitational Wave Signal for Quark Matter with Realistic Phase Transition. *Phys. Rev. Lett.* **2022**, *130*, 091404. [CrossRef]